

Introduction to biophysics

Bert Kappen,
Department of Biophysics
Radboud University Nijmegen

February 7, 2008

Contents

1	Preface	4
2	Introduction to neurons and the brain	5
2.1	Nerve cells	5
2.2	The nervous system	8
2.3	Some features of the cortex	12
2.4	Summary	18
2.5	Exercises	18
3	Electrical properties of cells	19
3.1	Ion channels	20
3.2	The Nernst equation	21
3.3	The Goldman equation	23
3.4	The Nernst-Planck equation	24
3.5	The Hodgkin-Katz experiments	27
3.5.1	The role of K^+	27
3.5.2	The role of Na^+	28
3.5.3	Permeability changes during action potential	30
3.6	Summary	33
3.7	Exercises	33
4	The Hodgkin-Huxley model of action potentials	36
4.1	The voltage clamp technique	36
4.2	Two types of voltage dependent ionic currents	36
4.3	The Hodgkin-Huxley model	43
4.3.1	The K^+ conductance	48
4.3.2	The Na^+ conductance	50
4.3.3	Action potentials	51
4.4	Spike propagation	53
4.4.1	Passive current flow	53
4.4.2	Spike propagation	57
4.4.3	Myelin	60
4.5	Summary	64
4.6	Exercises	64

5	Synapses	67
5.1	Introduction	67
5.2	Chemical synapses	67
5.3	The post-synaptic potential	68
5.4	Stochastic PSPs	72
5.5	Learning	74
5.6	Long term potentiation	77
5.7	Hebbian learning	78
	5.7.1 Ocular dominance	79
5.8	Summary	81
5.9	Exercises	81
6	Perceptrons	82
6.1	Threshold units	82
6.2	Linear separation	83
6.3	Perceptron learning rule	84
	6.3.1 Convergence of Perceptron rule	86
6.4	Linear units	88
	6.4.1 Gradient descent learning	89
	6.4.2 The value of η	90
6.5	Non-linear units	91
6.6	Multi-layered perceptrons	92
6.7	Summary	95
6.8	Exercises	95

1 Preface

This introductory course on biophysics introduces the principles of electrical excitability of cell membranes, which form the basis of all information processing in the nervous system. The course covers some of the classical results, such as cellular membranes, ionic currents, equilibrium behavior and action potentials. The course is intended for physics students and will therefore have an emphasis on physical modeling.

Section 2 is an introductory chapter, where I will give an overview of some of the basic anatomical properties of the nervous system and of nerve cells and discuss the spiking behavior of nerve cells and their functional relevance. In section 3, I will discuss the stationary behavior of the cell, such as the relation between ionic concentrations inside and outside the cell, the ionic currents and the membrane potential. In section 4, I will discuss the mechanism for action potential generation, spike propagation, linear cable theory and the role of myelin. In section 5, I will discuss synapses and some aspects of learning. In section 6, I will give a brief introduction to a class of popular neural networks, the (multi-layered) perceptrons.

Bert Kappen
Nijmegen, January 2007

2 Introduction to neurons and the brain

Perhaps the major reason that neuro science is such an exciting field is the wealth of fundamental questions about the human brain (and the rest of the nervous system) that remain unanswered. Such understanding entails unraveling the interconnections of large numbers of nerve cells, that are organized into systems and subsystems.

The fact that cells are the basic element of living organisms was recognized early in the nineteenth century. It was not until well into the twentieth century, however, that neuro scientists agreed that nervous tissue, like all other organs is made up of these fundamental units. Santiago Ramón y Cajal argued persuasively that nerve cells are discrete entities and that they communicate with one another by means of specialized contacts called synapses. The human brain is estimated to contain 100 billion neurons and several times as many supporting cells, called neuroglial cells.

2.1 Nerve cells

In most respects, the structure of neurons resembles that of other cells. Each cell has a cell body containing a nucleus, endoplasmic reticulum, ribosomes, Golgi apparatus, mitochondria, and other organelles that are essential to the function of all cells (see fig. 2). Specific for nerve cells, is their dendritic structure (see fig. 3. The dendrites (together with the cell body) provide sites for the synaptic contacts made by the terminals of other nerve cells and can thus be regarded as specialized for receiving information. The number of inputs that a particular neuron receives depends on the complexity of its dendrite and can range from 1 to about 100.000. The information from the inputs that impinge on the dendrites is 'read out' at the border of the cell body and the *axon*. The axon is an extension that may reach from a few hundred micrometers to a meter. Typical axons in the brain a a few millimeters long. Axons in the spinal cord are about a meter long. The axon carries electrical signals over such distances through *action potentials*, a self-generating electrical wave that propagates from the cell body to the end of the axon.

The information encoded by action potentials is passed on to the next cell by means of *synaptic transmission*. The arrival of the action potential causes the release of *neurotransmitters*, which in turn modify the electrical properties of the post-synaptic cell. The net effect is a change of the membrane

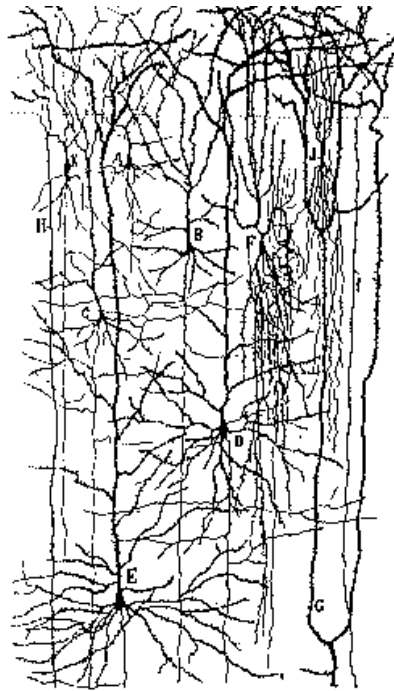


Figure 1: The brain consists of network of neurons (Ramón y Cajal, 1910). Shown is one of the original Golgi stain images of rat cortex. Only a small fraction of neurons are stained with this technique.

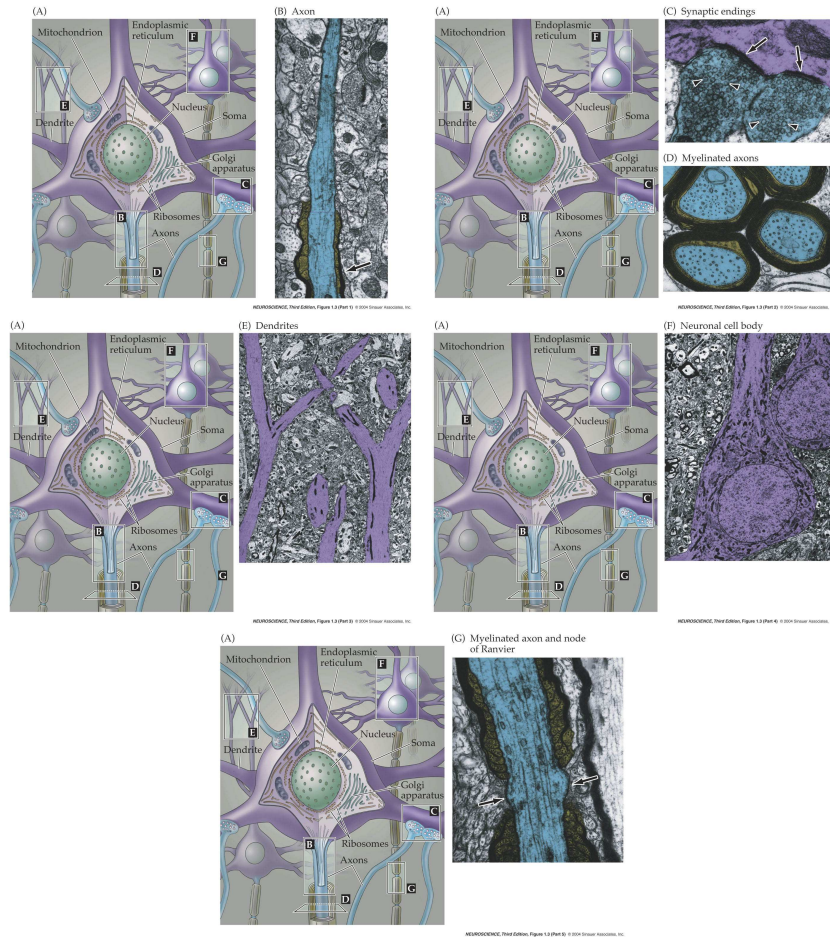


Figure 2: The major light and electron microscopical features of neurons. A) Diagram of nerve cells and their component parts. B) Axon initial segment (blue) entering a myelin sheath (gold). C) Terminal boutons (blue) loaded with synaptic vesicles (arrowheads) forming synapses (arrows) with a dendrite (purple). D) Transverse section of axons (blue) ensheathed by the processes of oligodendrocytes (gold). E) Apical dendrites (purple) of cortical pyramidal cells. F) Nerve cell bodies (purple) occupied by large round nuclei. G) Portion of a myelinated axon (blue) illustrating the intervals between adjacent segments of myelin (gold) referred to as nodes of Ranvier (arrows).

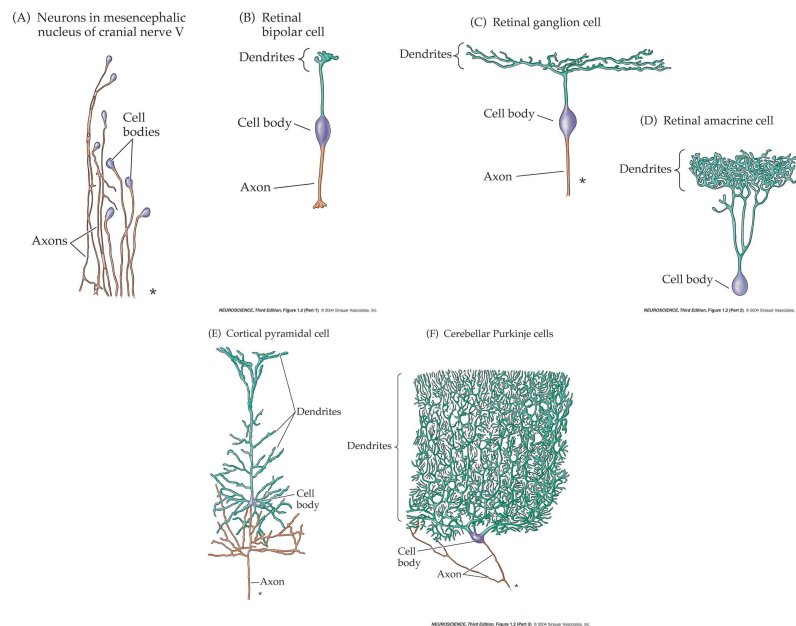


Figure 3: Cells stained with silver salts (Golgi stain). * indicates axon. a) muscle cell b-d) retinal cells e) Cortical pyramidal cell f) Cerebellar Purkinje cell

potential of the post-synaptic cell.

It is thought, that glia cells do not play a primary role in information processing in the brain. The different types of glia cells have two important functions. The *astrocytes* maintain in a variety of ways the appropriate chemical environment for the nerve cells. The *oligodendrocytes* or *Schwann cells* lay down a laminated wrapping called *myelin* around some, but not all, axons, which has important effects on the speed of action potential propagation.

2.2 The nervous system

The nervous system is traditionally divided into a central and peripheral component (see fig. 4). The peripheral system contains the sensory neurons, which receive information from the outside world, and the motor neurons, that connect to muscles and glands. Sensory information is processed in

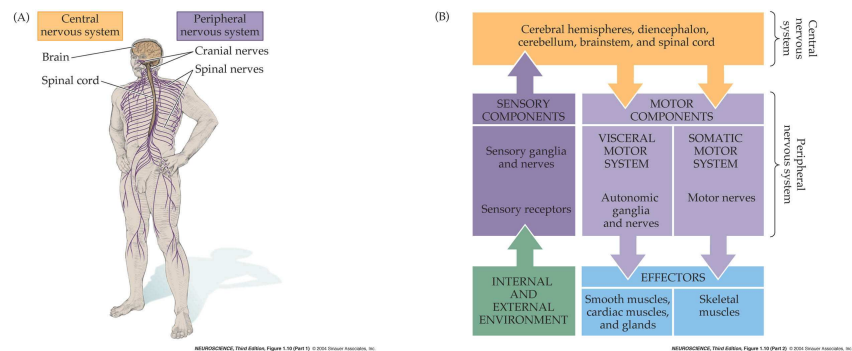


Figure 4: The major components of the nervous system and their functional relationships. A) The CNS (brain and spinal cord) and the PNS (spinal and cranial nerves). B) The peripheral nervous system receives sensory input and outputs motor commands. The central nervous system provides the 'mapping' from sensory input to motor output.

the brain, with the ultimate goal to generate the appropriate motor actions. Nerve cells that carry information toward the central nervous system are called *afferent neurons*, nerve cells that carry information away from the brain are called *efferent neurons*. Nerve cells that only participate in the local aspects of a circuit are called *inter-neurons*. The simple spinal reflex circuit in fig. 5 illustrates this terminology.

The central nervous system is usually considered to include seven basic parts (see fig. 6): the *spinal cord*; the *medulla*, the *pons* and the *midbrain* (collectively called the *brainstem*); the *cerebellum*; the *diencephalon* and the *cerebral hemispheres* (collectively called the *forebrain*).

The thalamus relays information to the cerebral cortex from other parts of the brain. Specialized substructures of the thalamus are engaged in motor functions and reproduction and hormone secretion. The brainstem contains structures, such as the *superior colliculus* that is involved in eye movement. The major function of the cerebellum is coordination of motor activity, posture and equilibrium. Like the cerebral cortex, the cerebellum is covered by a thin cortex. Another important area of the central nervous system is the hippocampus which is thought to be involved in the storage of episodic memories. It is not visible in fig. 6, since it is located centrally.

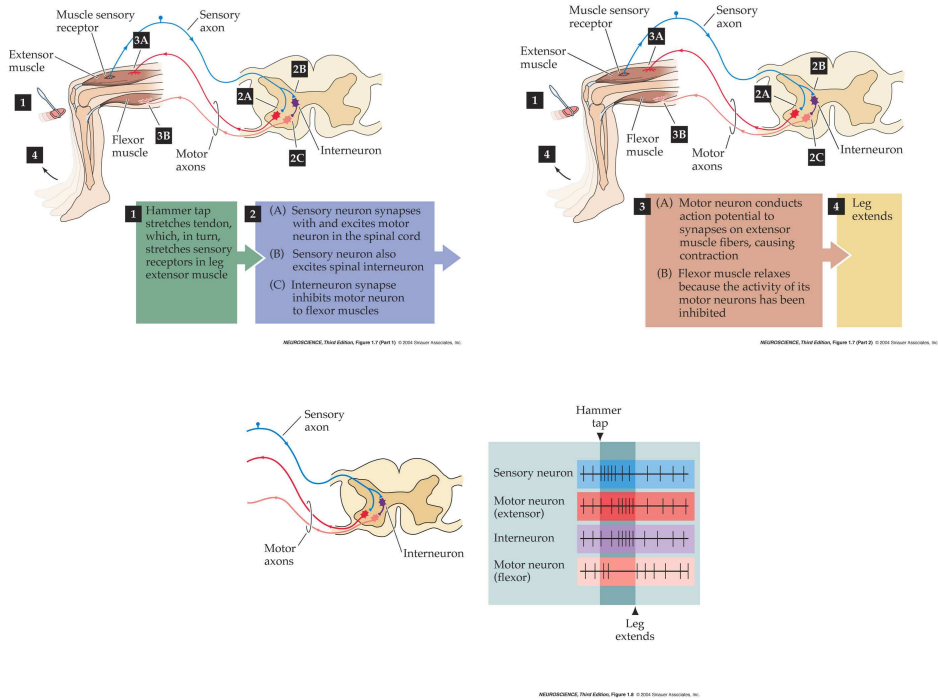


Figure 5: A simple reflex circuit, the knee-jerk response, illustrates several points about the functional organization of neural circuits. Stimulation of a muscle stretch receptor initiates action potentials that travel centrally along the afferent axons of the sensory neurons. This information stimulates spinal motor neurons by means of synaptic contacts. The action potentials generated in motor neurons travel peripherally in efferent axons, giving rise to muscle contraction. Bottom) Relative frequency of action potentials (indicated by individual vertical lines). Notice the modulatory effect of the interneuron.

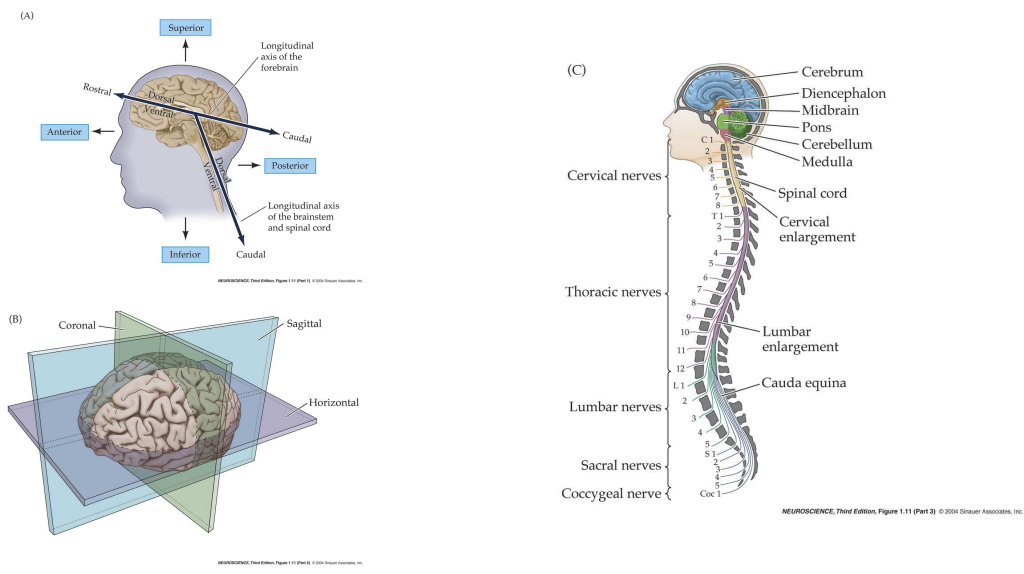


Figure 6: A) The terms anterior, posterior, superior, and inferior refer to the long axis of the body. B) The major planes of section used in cutting or imaging the brain. C) The subdivisions and components of the central nervous system.

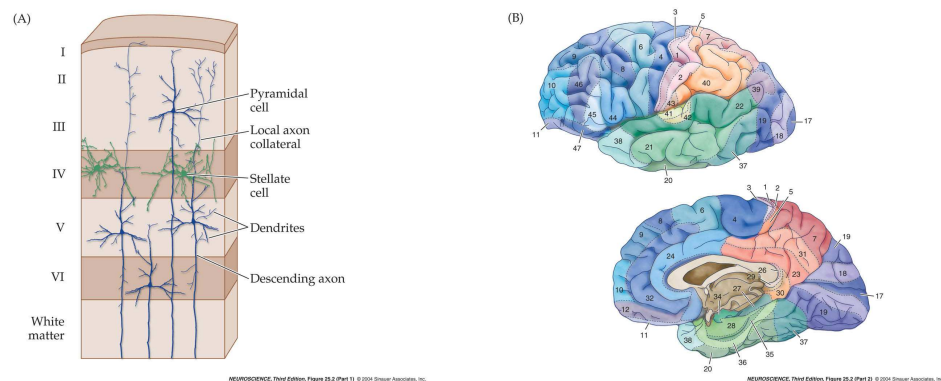
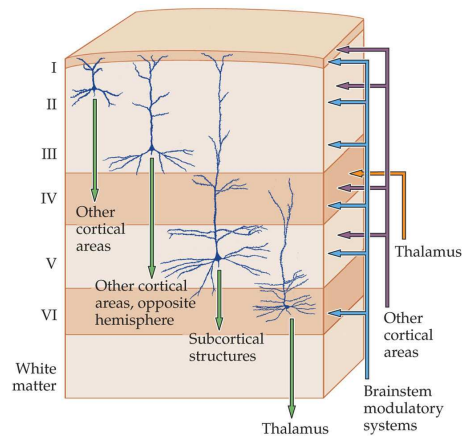


Figure 7: Structure of the human neocortex. A) summary of the cellular composition of the six layers of the neocortex. B) Based on variations in thickness, cell density and other histological features of the six neo-cortical laminae, the neocortex can be divided into areas (Brodmann 1909). These anatomical distinctions have later been shown to relate to different functions. Red indicates the primary motor cortex, blue the primary somatic sensory cortex, green the primary auditory cortex and yellow the primary visual cortex. All other Brodmann areas are considered association cortex.

2.3 Some features of the cortex

The cerebral hemispheres, also called the *cerebral cortex* are two convoluted sheets of neural tissue of about 2 mm thickness and spreads over about 11 dm² each. The sheets are connected through the *corpus callosum* (800 million fibers). The cortical sheet contains six layers that can be identified anatomically (fig. 7a). This structure of six layers is remarkably uniform through the cortex. Local differences has lead to the classification of the cortex into cortical areas (see fig. 7b).

The cortical tissue consists for about 80 % of pyramidal cells (fig. 3) and the remainder are so called inter-neurons. There are two types of pyramidal neurons, the *upper pyramidal neurons* lying in layers II and III and the *lower pyramidal neurons* which we find mainly in layer V. Both receive their input signals from *stellate cells*, which are inter-neurons lying in layer IV. The lower pyramidal neurons are output neurons; their axons make contact with the thalamus. The upper pyramidal neurons make distant connections with the pyramidal cells of other cortical areas. The six layer structure is schematically



NEUROSCIENCE, Third Edition, Figure 25.3 © 2004 Sinauer Associates, Inc.

Figure 8: Canonical neo-cortical circuitry. Green arrows indicate outputs to the major targets of each of the neo-cortical layers in humans; orange arrow indicates thalamic input (primarily to layer IV); purple arrows indicate input from other cortical areas: and blue arrows indicate input from the brainstem to each layer.

drawn in fig. 8.

Neurons in the sensory parts of the cortex, such as the visual, auditory or somatic sensory cortex, respond selectively to stimuli from the outside world. This gives rise to the notion of a *receptive field* of a neuron, which is the collection of all stimuli that elicit an electrical response in that neuron. In Fig. 9 we see an example of a somatosensory receptive field. The use of micro-electrodes to record action potential activity for different stimuli, provides a cell-by-cell analysis of the receptive field of each cell and the organization of topographic maps. In Fig. 10, we see an example of a visual receptive field. Some neurons in the visual cortex respond selectively to the orientation of a light bar. Each neuron has its preferred orientation.

Nearby pyramidal cells can make direct excitatory synaptic connections or indirect inhibitory connections by connecting to an inhibitory interneuron, which in turn connects to another pyramidal cell. The probability of connection is very high for nearby pyramidal neurons and drops off at about $30 \mu\text{m}$. Therefore, neurons within a *cortical column*, which is a cross-section of the cortical sheet of about this diameter, display strongly correlated ac-

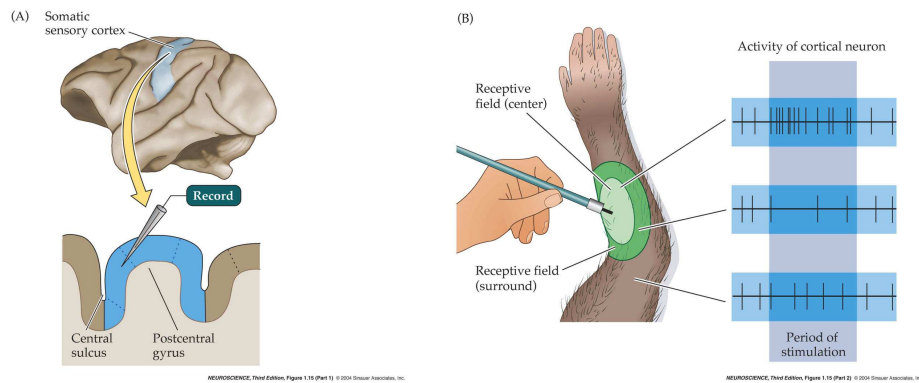


Figure 9: Single-unit electrophysiological recording from cortical pyramidal neuron, showing the firing pattern in response to a specific peripheral stimulus. A) Typical experimental set-up. B) Defining neuronal receptive fields.

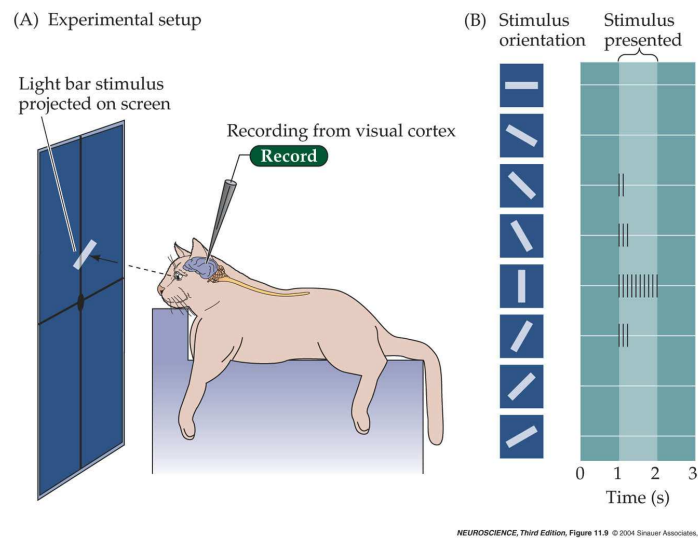


Figure 10: Neurons in the visual cortex respond selectively to oriented edges. A) An anesthetized cat focuses on a screen, where images can be projected; an extracellular electrode records the responses of neurons in the visual cortex. B) Neurons in the visual cortex typically respond vigorously to a bar of light oriented at a particular angle and weakly (or not at all) to other orientations.

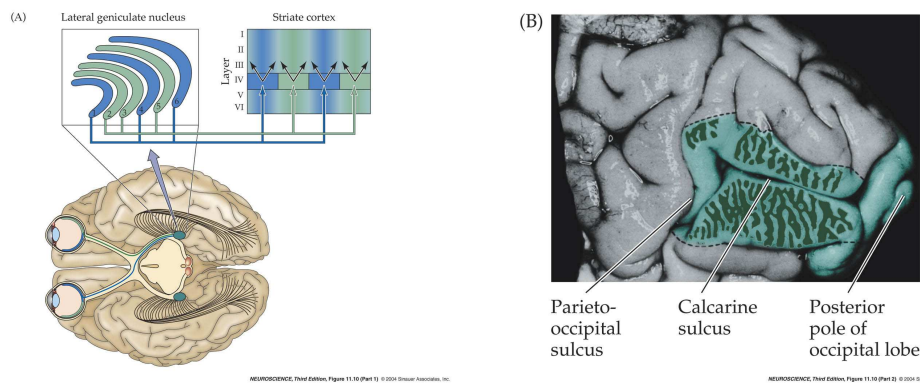


Figure 11: A) Ocular dominance stripes in LGN and layer IV primary visual cortex. B) Pattern of ocular dominance columns in human striate cortex.

tivity. The result is that nearby neurons have similar functional roles. An example is ocular dominance given in fig. 11. The lateral geniculate nucleus (LGN) receives inputs from both eyes, but this information is segregated in separate layers. In many species, including most primates, the inputs from the two eyes remain segregated in the ocular dominance columns of layer IV, the primary cortical target of LGN axons. Layer IV neurons send their axons to other cortical layers; it is at this stage that the information from the two eyes converges onto individual neurons.

Such correlated activity can also be measured in vivo. Fig. 12 shows that neurons in the same column have identical orientation preference. Neurons in nearby columns have similar orientation preference. Thus, this part of visual cortex displays a *topographical map*, meaning that stimulus features (in this case the orientation) are mapped continuously onto the spatial location in the cortex.

Cortical maps are found throughout the sensory cortices and motor cortex. Fig. 13 shows that nearby neurons in the auditory cortex respond preferentially to nearby frequencies. Typically, maps are deformed representations, that use more neurons to represent important regions. In fig. 14 shows the example of the somatotopic order in the human primary somatic sensory cortex.

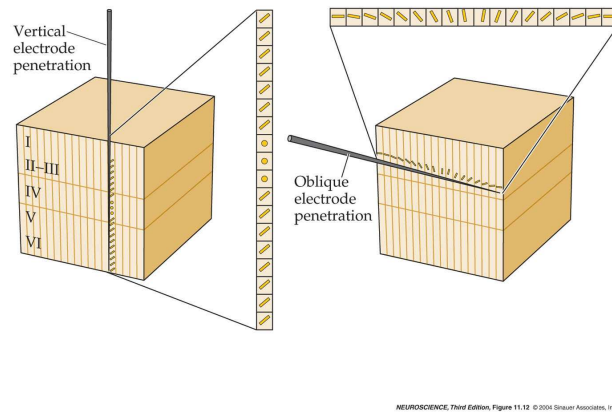


Figure 12: Columnar organization of orientation selectivity in the monkey striate cortex. Vertical electrode penetrations encounter neurons with the same preferred orientations, whereas oblique penetrations show a systematic change in orientation across the cortical surface.

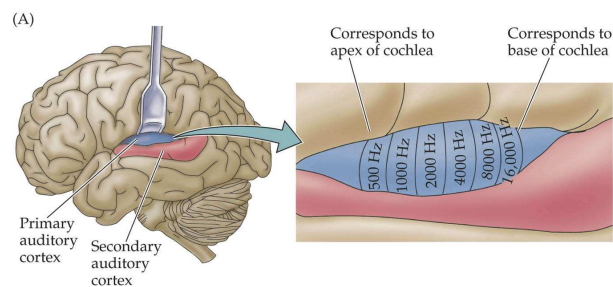
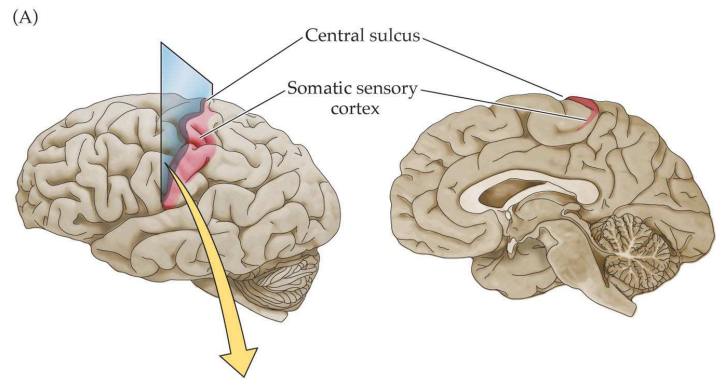
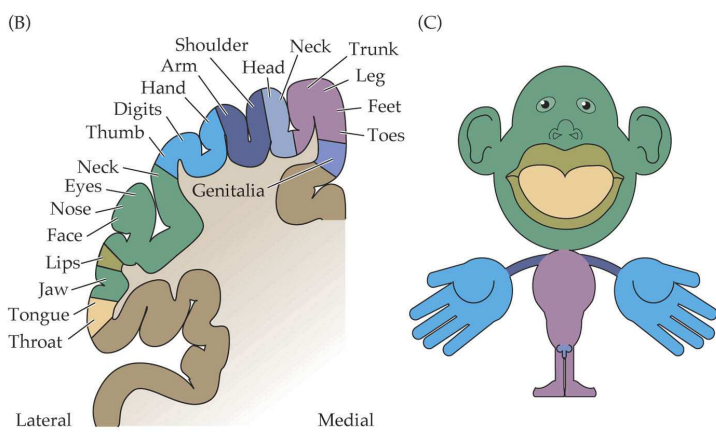


Figure 13: The human auditory cortex. A) Diagram showing the brain in left lateral view. The primary auditory cortex (A1) is shown in blue. B) The primary auditory cortex has a tonotopic organization.



NEUROSCIENCE, Third Edition, Figure 8.8 (Part 1) © 2004 Sinauer Associates, Inc.



NEUROSCIENCE, Third Edition, Figure 8.8 (Part 2) © 2004 Sinauer Associates, Inc.

Figure 14: Somatotopic order in the human primary somatic sensory cortex. A) approximate region of human cortex from which electrical activity is recorded following mechanosensory stimulation of different parts of the body. B) Somatotopic representation of the whole body. C) Cartoon of the homunculus constructed on the basis of such mapping. The amount of somatic sensory cortex devoted to hands and face is much larger than the relative amount of body surface in these regions.

2.4 Summary

Although the human brain is often discussed as if it were a single organ, it contains a large number of systems and subsystems. Various types of neurons in these systems are assembled into interconnected circuits that relay and process the electrical signals that are the basis of all neural functions. Sensory components of the nervous system supply information to the central nervous system about the internal and external environment. The integrated effects of central processing are eventually translated into action by the motor components. The material in this chapter is largely based on [1].

2.5 Exercises

1. Propose a neuron with its input dendritic tree connected to the retina, such that the neuron has the receptive field property as observed in figure 10.
2. Think about a neural network that may cause the ocular dominance patterns observed in figure 11.
 - (a) Consider the strength and sign of the forward connections from the eyes to the cortex.
 - (b) The lateral connections within the cortex are typically of the Mexican hat type: short range excitatory connections and long range inhibitory connections. Explain their role.
3. Suppose you were a neuron and you could only communicate with your fellow neurons through the emission of action potentials. How would you do it? Describe two ways and discuss their respective advantages and disadvantages.

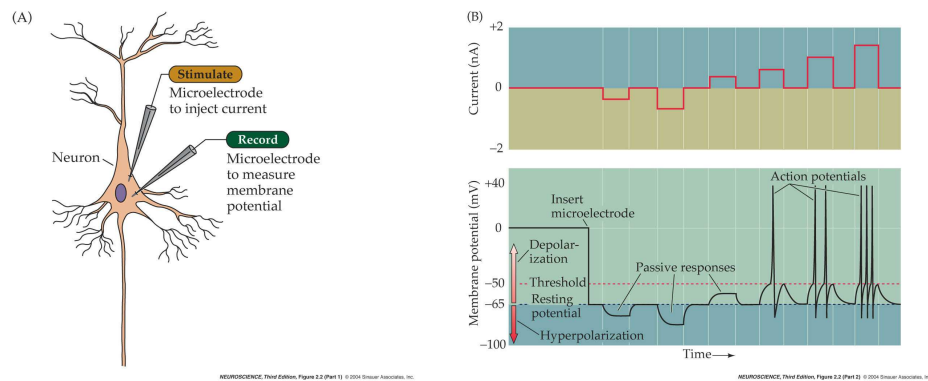
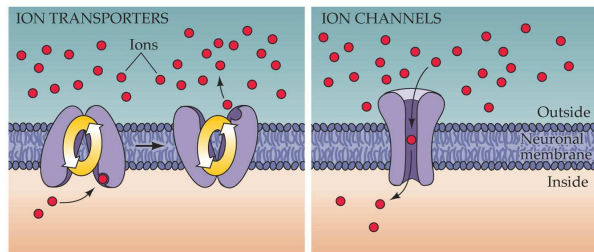


Figure 15: Recording passive and active electrical signals in a nerve cell.

3 Electrical properties of cells

Nerve cells generate electrical signals that transmit information. Neurons are not good conductors of electricity, but have evolved elaborate mechanisms for generating electrical signals based on the flow of ions across their membranes. Ordinarily, neurons generate a negative potential, called the resting membrane potential, that can be measured by intracellular recording. The action potential is a short spike in the membrane potential, making the membrane potential temporarily positive. Action potentials are propagated along the length of axons and are the fundamental electrical signal of neurons. Generation of both the resting potential and the action potential can be understood in terms of the nerve cell's selective permeability to different ions and the relative concentrations of these ions inside and outside the cell.

The best way to observe an action potential is to use an intracellular microelectrode to record directly the electrical potential across the neuronal membrane (fig. 15). Two micro-electrodes are inserted into a neuron, one of these measures the membrane potential while the other injects current into the neuron. Inserting the voltage-measuring microelectrode into the neuron reveals a negative potential, the resting membrane potential. Typical values are -60-80 mV. Injecting current through the current-passing microelectrode alters the neuronal membrane potential. Hyper-polarizing current pulses decrease the membrane potential and produce only passive changes in the membrane potential. Depolarizing currents increase the membrane potential.



NEUROSCIENCE, Third Edition, Figure 2.3 © 2004 Sinauer Associates, Inc.

Figure 16: Ion pumps and ion channels are responsible for ionic movements across neuronal membranes.

Small currents evoke a passive response. Currents that exceed a threshold value, evoke an action potential. Action potentials are active responses in the sense that they are generated by changes in the permeability of the neuronal membrane.

3.1 Ion channels

Electrical potentials are generated across the membranes of neurons (in fact of all cells) because (1) there are difference in the concentrations of specific ions across nerve cell membranes and (2) the membranes are selectively permeable to some of these ions (fig. 16). The ion concentration gradients are established by proteins known as *ion pumps*, which actively move ions into or out of cells against their concentration gradients. The selective permeability of membranes is due largely to *ion channels*, proteins that allow only certain kinds of ions to cross the membrane in the direction of their concentration gradients. Thus, channels and pumps basically work against each other, and in so doing they generate cellular electricity.

Membrane channels can open or close in response to changes in their direct vicinity, such as a change in the membrane potential, changes in the concentration of neurotransmitters, or sensory input. For instance, hair cells in the cochlea (inner ear) mechanically deform in response to sound, and this

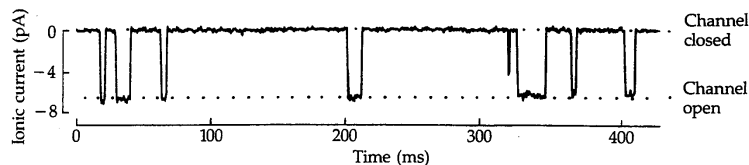


Figure 17: Open-shut gating of an ionic channel showing 8 brief openings. The probability of opening depends on many factors. At -140 mV applied membrane potential, one open channel passes 6.6 pA, corresponding to a flow of 4.1×10^7 ions per second.

mechanical deformation changes the permeability of certain channels. Channels open and close rapidly in a stochastic manner (fig. 17). The macroscopically observed permeability of the membrane is related to the probability that the channel is open.

3.2 The Nernst equation

Consider a simple system in which an imaginary membrane separates two compartments containing solutions of ions. Let both compartments contain an amount of potassium ions (K^+) and an equal amount of some negatively charged ions A^- , such that both compartments are electrically neutral. Suppose that the membrane is permeable only to potassium ions. If the concentration of K^+ on each side of the membrane is equal, then no electrical potential across it will be measured. However, if the concentration of K^+ is not the same on the two sides (and thus the concentrations of A^- differ as well, but these cannot move), then the potassium ions will flow down their concentration gradient and take their electrical charge with them as they go. Therefore, an electrical potential will be generated, which will drive K^+ ions in the reverse direction. An *electrochemical equilibrium* will be reached when the diffusive force equals the electromotive force (fig. 18). The positive and negative charge excess in both compartments will concentrate against the membrane (why?) like a capacitor. We thus conclude that the equilibrium potential difference will be an increasing function of the ratio of concentrations of K^+ in the two compartments.

The electrochemical equilibrium can be quantitatively described by the Boltzmann statistics, which states that the probability P to encounter a

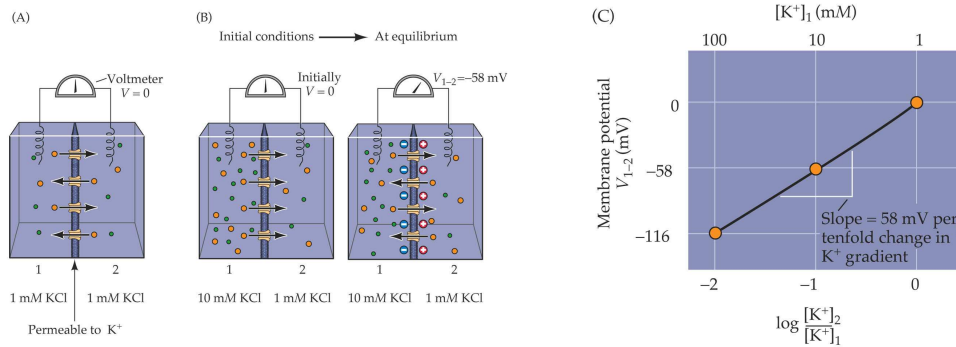


Figure 18: A-B) Electrochemical equilibrium due to selective permeability to K^+ ions. Concentration gradient drives K^+ ions to the right establishing a charge difference. In equilibrium the ionic current due to the concentration difference balances the current in the reverse direction due to the electrical potential difference. C) The relationship between the transmembrane concentration gradient and the membrane potential as predicted by the Nernst equation Eq. 1

system in equilibrium in a state with energy u is proportional to

$$P \propto \exp\left(-\frac{u}{kT}\right) = \exp\left(-\frac{U}{RT}\right)$$

with u the potential energy per ion, k is the Boltzmann constant and T is the absolute temperature. $U = N_A u$ is the potential energy per mole; $N_A = 6.022 \times 10^{23} \text{ mol}^{-1}$ is Avogadro's number; and $R = kN_A = 8.314 \text{ J mol}^{-1} \text{ K}^{-1}$ is the Gas constant.

The charged ions S that can move freely through the membrane can be in two states: in the left or right compartment, which we denote by l and r , respectively. The potential energy is proportional to the electric potential V and thus the potential energy per mole of an ion of valence z_S is given by

$$U_{l,r} = z_S e N_A V_{l,r} = z_S F V_{l,r}$$

with e the unit of electric charge and $F = eN_A = 9.648 \times 10^4 \text{ C mol}^{-1}$ is called the Faraday constant.

Thus, for a given electrical potentials V_l and V_r in the left and right compartment, we can compute the relative probability to encounter an S ion

left or right:

$$\frac{P_l}{P_r} = \frac{\exp(-z_S F V_l / RT)}{\exp(-z_S F V_r / RT)} = \exp\left(-\frac{z_S F}{RT}(V_l - V_r)\right)$$

The concentration of ions in the left and right compartment, $[S]_{l,r}$, is proportional to the probability $P_{l,r}$. We can invert the above expression and express the difference in electrical potential in terms of the concentrations:

$$V_{\text{Nernst}} = V_l - V_r = \frac{RT}{z_S F} \ln \frac{[S]_r}{[S]_l} \quad (1)$$

This expression is known as the Nernst equation and describes both the equilibrium concentration ratio when we apply an external potential difference, as well as the equilibrium potential difference when we consider the above system at fixed concentration differences. The Nernst potential depends on temperature, the concentration ratio and valence of the freely moving ions. In practice, it is often useful to replace the natural logarithm by the base-10 logarithm: $\ln = 2.3 \log_{10}$. Then

$$V_{\text{Nernst}} = \frac{1}{z_S} \log_{10} \left(\frac{[S]_r}{[S]_l} \right) \times 58 \text{mV}$$

at $T = 20^\circ\text{C}$.

For biological membranes, the K^+ concentration is typically much higher inside the cell than outside the cell. A typical ratio is $[\text{K}^+]_{\text{out}} : [\text{K}^+]_{\text{in}} = 1 : 10$, yielding a Nernst potential of -58 mV.

The number of ions that needs to flow to generate the electrical potential is very small (exercise). This means that the movement of ions required to reach the Nernst potential 1) hardly affects the neutrality of the intra- and extracellular media and 2) do not require much pumping by the ion pumps.

3.3 The Goldman equation

The Nernst equation accurately describes the relation between ion concentrations and the membrane potential, when only one type of ion can move through the membrane. In reality, many types of ions are present in the intra and extracellular medium, each of which has its own permeability. Some realistic numbers are given in table 1. For instance, imagine what would happen if the intracellular K^+ and Na^+ concentrations are 100 mM and 10

Ion	Intracellular	Extracellular
Squid axon		
K ⁺	400	20
Na ⁺	50	440
Cl ⁻	40-150	560
Ca ²⁺	0.0001	10
Mammalian neuron		
K ⁺	140	5
Na ⁺	5-15	145
Cl ⁻	4-30	110
Ca ²⁺	0.0001	1-2

Table 1: Extracellular and intracellular ion concentrations in millimole per liter (mM).

mM, respectively and the extracellular concentrations of K⁺ and Na⁺ are reversed: 10 mM for K⁺ and 100 mM for Na⁺. If the membrane would be only permeable to K⁺, the membrane potential would be -58 mV. If the membrane would be only permeable to Na⁺, the membrane potential would be +58 mV. What will happen if the membrane is partially permeable for both ions?

For the case most relevant to neurons, in which K⁺, Na⁺ and Cl⁻ are the primary permeant ions, the general solution, called the *Goldman equation*, was developed by David Goldman in 1943:

$$V = \log_{10} \left(\frac{P_{K^+}[K^+]_r + P_{Na^+}[Na^+]_r + P_{Cl^-}[Cl^-]_l}{P_{K^+}[K^+]_l + P_{Na^+}[Na^+]_l + P_{Cl^-}[Cl^-]_r} \right) \times 58\text{mV} \quad (2)$$

where V is the equilibrium voltage across the membrane, and the $P_i, i = K^+, Na^+, Cl^-$ are the permeabilities of the three types of ions. We see that in the case that the membrane is only permeable to one ion, the Goldman equation reduces to the Nernst equation. In the following subsection, we will derive the Goldman equation.

3.4 The Nernst-Planck equation

Consider a membrane of thickness a and let $x = 0$ to $x = a$ denote the outside and inside of the membrane, respectively. Let the electrical potential be $V_{\text{out}} = V(0) = 0$ and $V_{\text{in}} = V(a) = V$. Let us assume that we have

a number of different ions, labeled by i , each with its own concentration $C_i(x)$ and valence z_i . The extracellular and intracellular concentrations are denoted by

$$[C_i]_{\text{out}} = C_i(0), \quad [C_i]_{\text{in}} = C_i(a) \quad (3)$$

Due to the potential difference and the concentration differences, ions will flow through the membrane. The electric force per ion of type i is $-z_i e \frac{dV(x)}{dx}$. The number of ions per liter is $N_A C_i(x)$, with $C_i(x)$ in units of mol per liter. Therefore, the electric force per unit volume is

$$-z_i C_i(x) F \frac{dV(x)}{dx}$$

The diffusive force on ion i per unit volume is proportional to the concentration gradient as well as the absolute temperature. Multiplying by the Gas constant gives the diffusive force

$$-RT \frac{dC_i(x)}{dx}$$

in units of Newton per liter.

The force on the ions is the sum of the electric and diffusive force and results in a movement of the ions proportional to the mobility u_i of the ions. The mobility will be soon related to the specific permeability of the membrane to each of the ions. The direction of movement is in the direction of the force, but the direction of charge depends again on the valence. Therefore, the current for ions i is:

$$I_i = u_i z_i \left(-RT \frac{dC_i(x)}{dx} - z_i C_i(x) F \frac{dV(x)}{dx} \right) \quad (4)$$

Eq. 4 is a differential equation in $C_i(x)$, given the values of I_i and the electric potential $V(x)$ as a function of x and is known as the Nernst-Planck equation. Note, that while the ion concentration and the electric potential depend on location x , the current is independent of x . This is a consequence of the conservation of charge and the fact that we are in one dimension.

To solve Eq. 4, we should also describe how $V(x)$ depends on the charge distributions $C_i(x)$ using Gauss' law. Instead, we will make the simplifying assumption that the membrane potential changes linearly from the outside to the inside of the membrane, $dV/dx = V/a$ for $0 < x < a$. Then we can

easily solve Eq. 4 with the boundary conditions Eq. 3 (exercise 4a). The result is

$$I_i = \frac{-u_i z_i^2 FV [C_i]_{\text{out}} - [C_i]_{\text{in}} \exp\left(z_i \frac{FV}{RT}\right)}{a \left(1 - \exp\left(z_i \frac{FV}{RT}\right)\right)} \quad (5)$$

Eq. 5 predicts the ion current that results from an electrical potential difference together with a ionic concentration difference. The current as a function of the voltage behaves as a rectifier, where the effective resistance for current in one direction is different from the other direction. The typical shape of I_i as a function of V is shown in fig. 19. The cause for this is the difference in ionic concentrations on the different sides of the membrane. Indeed, from Eq. 5 we see that when $[C_i]_{\text{out}} = [C_i]_{\text{in}}$, the current voltage relation is linear as in Ohms law.

We now consider the case where we have various ion concentrations inside and outside the cell. If we consider Eq. 5 for $i = \text{K}^+, \text{Na}^+, \text{Cl}^-$ The total current is given by

$$I = I_{\text{K}^+} + I_{\text{Na}^+} + I_{\text{Cl}^-} = \frac{-FV w - ye^{FV/RT}}{a \left(1 - e^{FV/RT}\right)} \quad (6)$$

with

$$\begin{aligned} w &= u_{\text{K}^+} [\text{K}^+]_{\text{out}} + u_{\text{Na}^+} [\text{Na}^+]_{\text{out}} + u_{\text{Cl}^-} [\text{Cl}^-]_{\text{in}} \\ y &= u_{\text{K}^+} [\text{K}^+]_{\text{in}} + u_{\text{Na}^+} [\text{Na}^+]_{\text{in}} + u_{\text{Cl}^-} [\text{Cl}^-]_{\text{out}} \end{aligned}$$

In the stationary case, there will be no net movement of charge and $I = \frac{dQ}{dt} = 0$. Then we can solve for the membrane potential V in terms of the various concentrations inside and outside the cell. The solution is given by the Goldman Eq. 2 (exercise).

For small currents, we can linearize Eq. 6 around the stationary solution. The result is (exercise)

$$G = \frac{dI}{dV}_{V=V_0} = \frac{F}{a} \frac{wy}{y-w} \log \frac{w}{y} \quad (7)$$

$$I \approx G(V - V_0) + \mathcal{O}((V - V_0)^2) \quad (8)$$

G has units of Ω^{-1} per liter and is called the conductance and is the inverse resistance. V_0 the equilibrium membrane potential given by the Goldman equation.

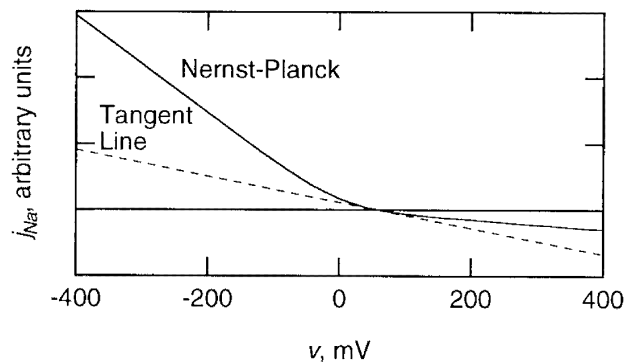


Figure 19: Current voltage relation Eqs. 5 and 6 as predicted by the Nernst-Planck equation under the assumption of constant electric force. The difference in slope for positive and negative voltage is due to the concentration differences inside and outside the membrane.

3.5 The Hodgkin-Katz experiments

3.5.1 The role of K^+

Once the ion concentration gradients across various neuronal membranes are known, the Nernst equation can be used to calculate that the equilibrium potential for K^+ is more negative than of any other major ion. Since the resting membrane potential of the squid neuron is approximately -65 mV, K^+ is the ion that is closest to electrochemical equilibrium when the cell is at rest. This fact suggests that the resting membrane is more permeable to K^+ than to the other ions listed in table 1.

It is possible to test this hypothesis, by asking what happens to the resting membrane potential as the concentration of K^+ outside the cell is altered. Assuming that the internal K^+ concentration is unchanged during the experiment and that the membrane is effectively impermeable to all other ions, the Nernst equation predicts that the membrane potential varies linearly with the logarithm of the external K^+ concentration. The experiment was performed by Alan Hodgkin and Bernard Katz in 1949 on a living squid neuron. The results are shown in fig. 20. When the external K^+ concentration is raised to the level of the internal concentration, the membrane potential is indeed found to be approximately zero.

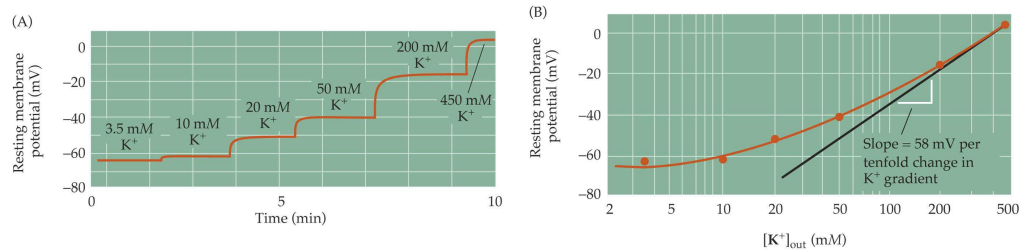


Figure 20: Experimental evidence that the resting membrane potential of a squid giant axon is determined by the K^+ concentration gradient across the membrane. A) In creasing the external K^+ concentration makes the resting membrane potential more positive. B) Resting membrane potential versus K^+ concentration as found experimentally and as predicted by the Nernst equation.

For small K^+ concentrations, we observe a discrepancy between the experimental results and the predictions of the Nernst equation. This difference can be accounted for by using the more accurate Goldman equation (exercise).

In summary, Hodgkin and Katz showed that the negative resting potential of neurons arises because 1) the membrane is more permeable to K^+ than to any other ions and 2) there is more K^+ inside the neuron than outside. The permeability to K^+ is the result of K^+ -permeable channels that are open when the neuron is at rest. The concentration difference is the result of membrane pumps. Subsequent studies have shown that this basic picture is generally valid on all neurons.

3.5.2 The role of Na^+

During an action potential the membrane resting potential reverses from negative to positive (fig. 15). What causes this? Given the data presented in table 1, one can use the Nernst equation to calculate that the equilibrium potential for Na^+ (E_{Na^+}) is positive. Thus, if the membrane were to become highly permeable to Na^+ , the membrane potential would approach E_{Na^+} .

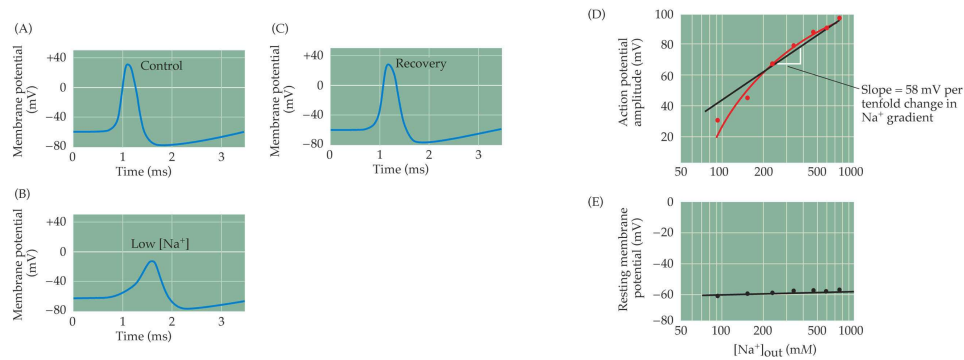


Figure 21: A-C) The external sodium concentration affects the size and rise time of the action potential (squid giant axon). D) Linear relationship between the amplitude of the action potential and the log of the Na⁺ concentration. E) Na⁺ concentration does not affect the resting membrane potential.

Hodgkin and Katz tested the role of Na⁺ in generating the action potential by asking what happens to the action potential when Na⁺ is removed from the external medium. They found that lowering the external Na⁺ concentration reduces both the rate of rise and the peak amplitude (fig. 21), with a more-or-less linear relationship between the amplitude of the action potential and the log of the Na⁺ concentration. Indeed, from the Nernst equation for Na⁺ we obtain when we change the external Na⁺ concentration from [Na⁺]_{out} to [Na⁺]_{out}'

$$V'_{\text{Na}^+} - V_{\text{Na}^+} = \frac{RT}{F} \ln \frac{[\text{Na}^+]_{\text{out}}'}{[\text{Na}^+]_{\text{in}}} - \frac{RT}{F} \ln \frac{[\text{Na}^+]_{\text{out}}}{[\text{Na}^+]_{\text{in}}} = \frac{RT}{F} \ln \frac{[\text{Na}^+]_{\text{out}}'}{[\text{Na}^+]_{\text{out}}}$$

In contrast, the external Na⁺ concentration has very little effect on the resting membrane potential. Thus, they concluded that the resting membrane is only slightly permeable to Na⁺ and then becomes very permeable to Na⁺ during the action potential. This temporary increase in Na⁺ permeability results from the opening of Na⁺ selective channels that are essentially closed in the resting state.

The fact that an action potential is accompanied with an increase of the conductance was earlier demonstrated by Cole and Curtis in 1939 (see fig. 22), but they did not identify the specific role of Na⁺ channels.

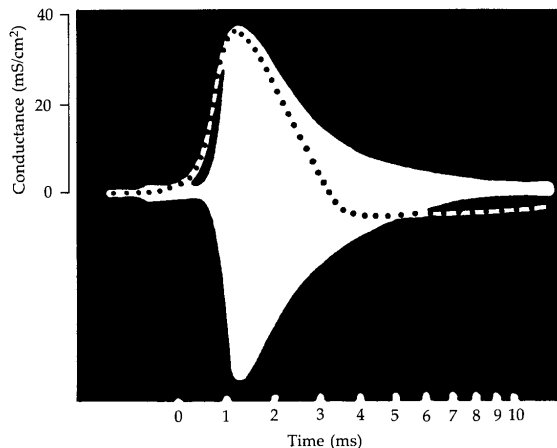


Figure 22: Conductance increase in excitation in squid giant axon. White band is the conductance, Dashed line is the action potential (Cole and Curtis 1939).

The time the membrane potential is near E_{Na^+} is brief because the increased membrane permeability to Na^+ is short-lived. The membrane potential rapidly re-polarizes and after this falling phase there is a transient undershoot, due to an increase in the K^+ permeability of the membrane, making the membrane even more permeable to K^+ than at rest.

3.5.3 Permeability changes during action potential

In the foregoing, we have not made any quantitative assumptions about the relative permeabilities of the membrane to sodium and potassium. The resting membrane has been considered as more permeable to potassium than sodium, and this condition was regarded as reversed during activity. It is natural to inquire, whether any limit can be set to the degree of selective permeability actually present in the resting and active membranes. Some light can be thrown on this problem if the observed potentials are compared with those predicted by the Goldman equation Eq. 2

There are many reasons for supposing that this equation is no more than a rough approximation, and it clearly cannot give exact results if ions enter into chemical combination with carrier molecules in the membrane or if ap-

preciable quantities of current are transported by ions other K^+ , Na^+ or Cl^- . But because of its simplicity, and because it reduces to the correct Nernst equation if only one of the ion permeabilities dominates, Hodgkin and Katz used it anyway.

In the physiological condition of the axon that they used, the internal ion concentrations were the following:

$$[K^+]_i = 345mM, \quad [Na^+]_i = 72mM, \quad [Cl^-]_i = 61mM$$

The experimental data against which the Goldman equation was tested are summarized in Table 2, which shows the average change in membrane potential produced by considering various external ion concentrations. It is seen, that there is reasonable agreement between all the results obtained with resting nerve and those predicted by the theory for $P_K^+ : P_{Na}^+ : P_{Cl}^- = 1 : 0.04 : 0.45$. These coefficients were obtained by trial and error. The value of the resting potential predicted on the basis of these values is 59 mV, while the observed resting potential averaged 48 mV. The difference is due to a liquid junction potential of 11 mV between sea water and axoplasm.

The peak of the action potential can be calculated if values are assumed for the relative permeabilities of the active membrane to sodium, potassium and chloride ions: with $P_K^+ : P_{Na}^+ : P_{Cl}^- = 1 : 20 : 0.45$ an action potential of -49 mV is obtained, which is roughly in agreement with the experimental value -40 mV. These values of the permeabilities may be used to predict the changes in potential when the external ion concentrations are changed in solutions A-I and are in reasonable agreement with the observed values.

The third block of numbers in Table 2 gives the changes in membrane potential recorded during the hyper-polarization of the action potential. In this condition the nerve is in a refractory state. Hodgkin and Katz assumed that the sodium permeability is reduced to zero and that it does not recover its normal value until the end of the relative refractory period. Using $P_K^+ : P_{Na}^+ : P_{Cl}^- = 1.8 : 0 : 0.45$ give good agreement between the Goldman equation and the observed values.

TABLE 7.

State of nerve	Solution	Composition of test solution			Change in membrane potential on substituting test solution for sea water or artificial sea water		Permeability coefficients used in calculation		
		K mm.	Na mm.	Cl mm.	Observed mV.	Calculated mV.	P_K	P_{Na}	P_{Cl}
Resting	A	0	465	587	+ 3	+ 5	1	0.04	0.45
	B	15	450	587	- 2	- 2			
	C	20	445	587	- 4	- 4			
	D	7	324	384	0	+ 1			
	E	5	227	270	+ 2	+ 2			
	F	3	152	180	+ 2	+ 2			
	G	2	91	108	+ 4	+ 3			
	H	10	573	658	+ 1	0			
	I	10	711	796	- 2	0			
Active (peak of spike)	A	0	465	587	+ 1	- 1	1	20	0.45
	B	15	450	587	+ 1	0			
	C	20	445	587	+ 5	- 1			
	D	7	324	384	+ 9	+ 8			
	E	5	227	270	+21	+16			
	F	3	152	180	+44	+25			
	G	2	91	108	+59	+38			
	H	10	573	658	- 3	- 5			
	I	10	711	796	- 9	- 10			
Refractory (maximum of positive phase)	A	0	465	587	+13	+12	1.8	0	0.45
	B	15	450	587	- 6	- 5			
	C	20	445	587	- 10	- 9			
	D	7	324	384	+ 1	+ 1			
	E	5	227	270	+ 4	+ 2			
	F	3	152	180	+ 4	+ 3			
	G	2	91	108	0	+ 3			
	H	10	573	658	+ 1	+ 1			
	I	10	711	796	0	+ 3			
Membrane potential at rest in sea water				+48 + J	+59	As above			
Membrane potential at height of activity in sea water				-40 + J	-38				
Membrane potential at maximum of positive phase				+62 + J	+74				
Action potential in sea water				88	97				
Positive phase in sea water				14	15				

Solutions A, B and C were tested against an artificial sea-water solution containing 10 mm-K, 455 mm-Na, 587 mm-Cl. Solutions D-I were tested against sea water containing approximately 10mm-K, 455 mm-Na, 540 mm-Cl. Calculated potentials were obtained from equation 4 using values of $(K)_i = 345$ mm., $(Na)_i = 72$ mm., $(Cl)_i = 61$ mm. J is the liquid junction potential between the axoplasm and the sea water in the microelectrode.

5-9

Table 2: (From [2]) showing the change in membrane potential when the external concentrations of potassium, sodium and chlorine are changed under three conditions: at rest, during the peak of the action potential, and after the action potential. In each of these three conditions, the relative permeabilities of the three ions are adjusted to obtain agreement between the experimental results and those obtained by the Goldman equation Eq. 2. It shows that Ca^{2+} permeability is highly increased during the action potential. Note, that Hodgkin and Katz used a definition of the membrane potential that is minus the modern definition used throughout this reader.

3.6 Summary

The resting membrane potential is the result of different ions concentrations inside and outside the cell and the specific permeability of the membrane to different ions. The relation between ionic concentrations and equilibrium membrane potential is described by the Nernst equation for single ions and by the Goldman equation for multiple ions. At rest, the nerve cell is mainly permeable to K^+ ions resulting in a negative resting membrane potential. During the action potential, the Na^+ permeability dominates and the membrane potential reverses sign. The increased Na^+ permeability is short, resulting in a short voltage spike. After the action potential, the Na^+ permeability is reduced to zero, leading to a hyper-polarization of the membrane. During this so-called refractory period no new action potentials can be generated.

Although we have identified the ions that flow during an action potential, we did not establish how the membrane is able to change the ionic permeability. As we will see in the next chapter, it is the neural membrane potential itself that affects the membrane permeability.

The discussion of the ion channels, Nernst equation and Goldman equation is based on [1]. The derivation of the Nernst-Planck and Goldman equations and the description of the Hodgkin-Katz experiment is from [2].

3.7 Exercises

1. Explain why in Fig. 18, all excess charge accumulates near the membrane on both sides.
2. Consider the membrane of a neuron as a capacitor that can hold an amount of charge proportional to the potential difference: $Q = CV$. V is the potential difference between outside and inside of the cell and is measured in Volt, Q the charge on either side of the membrane and is measured in Coulomb per cm^2 (C/cm^2) and C is the capacitance measured in Farad per cm^2 (F/cm^2).
 - (a) Compute the capacitance, approximating the membrane by a parallel plate capacitor:

$$C = \frac{\epsilon\epsilon_0 A}{d}$$

ϵ_0 is the polarizability of free space and is $8.85 \times 10^{-12} \text{CV}^{-1}\text{m}^{-1}$. The dielectric constant of hydrocarbon chains is $\epsilon = 2.1$. The

thickness of the membrane is 2.3 nm.

- (b) Compute the number of charged ions that are required to maintain the Nernst potential at 58 mV.
3.
 - (a) What would happen to the Nernst potential if in the experiment of fig. 18 the K^+ ions were replaced by Na^+ ?
 - (b) What would happen to the Nernst potential if in the experiment of fig. 18 the K^+ ions were replaced by Ca^{2+} and the membrane would be selectively permeable for Ca^{2+} ?
 - (c) What would happen to the Nernst potential if in the experiment of fig. 18 the K^+ ions were replaced by Cl^- and the membrane would be selectively permeable for Cl^- ?
4.
 - (a) Solve the Nernst-Planck Eq. 4 for constant I_i under the boundary conditions Eq. 3 and assuming that the electrical potential changes linearly with x within the membrane: $V(x) = Vx/a$. Derive Eq. 5.
 - (b) Show the rectification behavior of Eq. 5 by computing its behavior for large positive and negative V .
5. Derive the Goldman equation Eq. 2 for the case most relevant to neurons, in which K^+ , Na^+ and Cl^- are the primary permeant ions. Use the current voltage relations Eq. 5 and the additional condition that no net charge is flowing, $\sum_i I_i = 0$,
6. Explain the deviation between the experimental curve in fig. 20 and the theoretical prediction by the Nernst equation in terms of the Goldman equation Eq. 2
7.
 - (a) Derive Eq. 7 from Eq. 6
 - (b) Show that the conductance increases when ion concentrations increase. Explain this effect in words.
8. The Nernst-Planck equations Eq. 5 and 6 relate the current to membrane voltage and ion concentrations. In this exercise, we compare experimental values with those found by Eq. 5 and 6.
 - (a) Some experimental measurement on the squid axon in rest shows an average increase of the intracellular Na^+ of 50 mM and an average decrease of the intracellular K^+ of 72 mM during a period of

3 hours. Express these findings in flow of ions per second through a surface of 1 cm^2 , assuming a cylindrical axon with diameter of $500 \text{ }\mu\text{m}$.

- (b) Eq. 5 gives the individual currents in terms of the experimentally accessible quantities: the ion concentrations and the membrane potential. The unknown quantity is the ion mobility u_i . Use the equation for the conductivity in the Goldman equilibrium Eq. 7 to write Eq. 5 for K^+ and Na^+ such that it involves only permeability ratios of the various ions and the membrane conductance G .
- (c) Compute the theoretical value for I_{K^+} and I_{Na^+} given the following values. The internal ion concentrations are $[\text{K}^+]_{\text{in}} = 345 \text{ mM}$, $[\text{Na}^+]_{\text{in}} = 72 \text{ mM}$, $[\text{Cl}^-]_{\text{in}} = 61 \text{ mM}$. The external ion concentrations are $[\text{K}^+]_{\text{out}} = 10 \text{ mM}$, $[\text{Na}^+]_{\text{out}} = 455 \text{ mM}$, $[\text{Cl}^-]_{\text{out}} = 540 \text{ mM}$. The permeability ratios when the membrane is at rest are $u_{\text{K}^+}^+ : u_{\text{Na}^+}^+ : u_{\text{Cl}^-}^- = 1 : 0.04 : 0.45$. The temperature is 20°C ($\frac{RT}{F} = 25.26 \text{ mV}$) and membrane resistance is $1000 \text{ }\Omega \text{ cm}^2$.

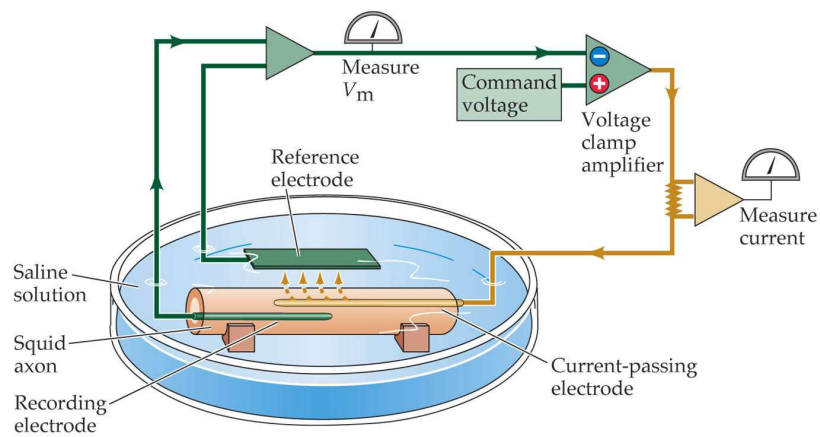
4 The Hodgkin-Huxley model of action potentials

4.1 The voltage clamp technique

This technique was invented by Kenneth Cole in 1940s. The device is called a voltage clamp because it controls, or clamps, membrane potential at any level desired by the experimenter (see fig. 23). This electronic feedback circuit holds the membrane potential at the desired level, even in the face of permeability changes that would normally alter the membrane potential. Also, the device permits the simultaneous measurement of the current needed to keep the cell at a given voltage. Therefore, the voltage clamp technique can indicate how the membrane potential influences ionic current flow across the membrane. The most popular contemporary version of the voltage clamp is the patch clamp technique (fig. 23E), which has a resolution high enough to measure the minute electrical currents flowing through a single ion channel (fig. 17)

4.2 Two types of voltage dependent ionic currents

In the late 1940s, Alan Hodgkin and Andrew Huxley used the voltage clamp technique to work out the permeability changes underlying the action potential. They chose to use the giant neuron of the squid because its large size (up to 1 mm in diameter) allowed insertion of the electrodes necessary for voltage clamping. To investigate the voltage dependent permeability of the membrane they asked whether ionic currents flow across the membrane when its potential is changed. Fig. 24A illustrates the currents produced by a squid axon when its membrane potential is hyper-polarized from the resting level of -65 mV to -130 mV. The initial response of the axon results from the redistribution of charge across the membrane. This capacitive current is nearly instantaneous, ending within a fraction of a millisecond. Aside from this event, very little current flows when the membrane is hyper-polarized. However, when the membrane potential is depolarized from -65 mV to 0 mV, the response is quite different (fig. 24B). The axon produces a rapidly rising inward ionic current, which later changes into an outward current. This complicated relation between voltage and current suggests that the membrane permeability is indeed voltage dependent (exercise).



NEUROSCIENCE, Third Edition, Chapter 3, Box A © 2004 Sinauer Associates, Inc.

Figure 23: 1) One internal electrode measures membrane potential and is connected to the voltage clamp amplifier. 2) Amplifier compares membrane potential to the desired potential. 3) When different, the amplifier injects current into the axon through a second electrode, and is measured (4).

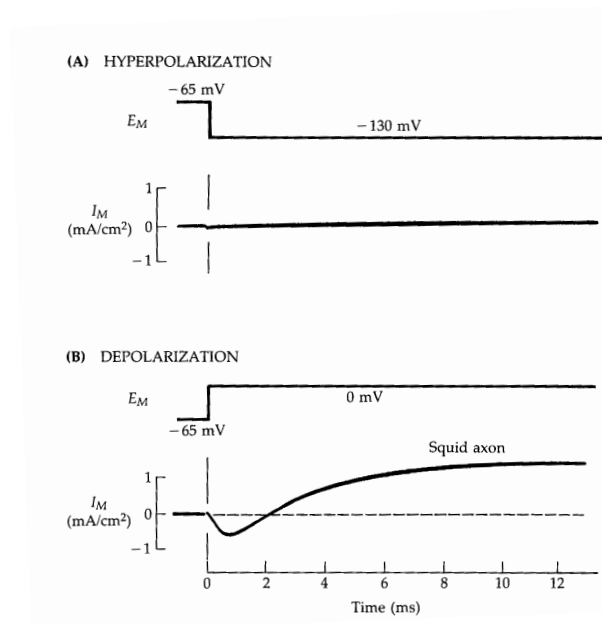


Figure 24: Current flow across a squid axon membrane during a voltage clamp experiment. A) A 65 mV hyper-polarization produces only a brief capacitive current. B) A 65 mV depolarization produces in addition a longer lasting current that initially flows inward and later flows outward [3].

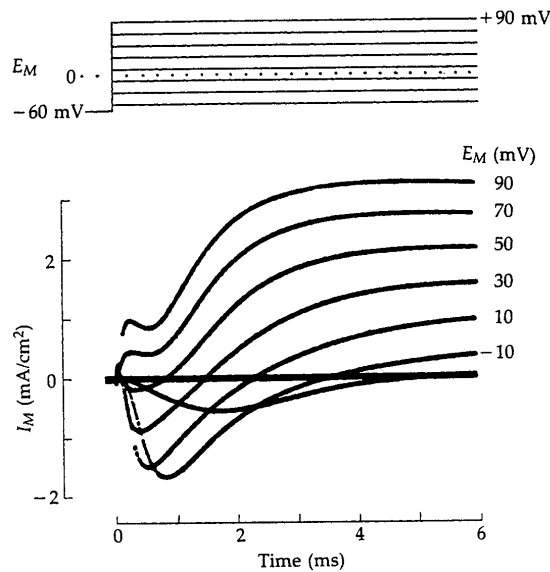


Figure 25: A squid giant axon membrane is stepped under voltage clamp from a holding potential of -60 mV to potentials ranging in 20 mV steps from -10 to +90 mV. Successive current traces have been superimposed [3].

Fig. 25 shows how the transient inward current and the sustained outward current depend on the clamp potential. Increasing the clamp potential from the resting value first shows an increase in the magnitude of the inward current up to approximately 0 mV, but this current decreases as the potential is depolarized further. In contrast, the late current increases monotonically with increasingly positive membrane potentials.

These different responses to membrane potential can be seen more clearly when the magnitudes of the two current components are plotted as a function of membrane potential (fig. 26). Note, that the early inward current becomes zero when the membrane is clamped at +52 mV. For the squid axon studied by Hodgkin and Huxley, the external Na^+ concentration is 440 mM and the internal Na^+ concentration is 50 mM. The corresponding Nernst potential for Na^+ (see section 3.2) is computed as +55 mV. This equilibrium potential is by definition the potential at which there is no net Na^+ current across the membrane. The proximity of these two values suggests that the inward transient current is caused by Na^+ ions.

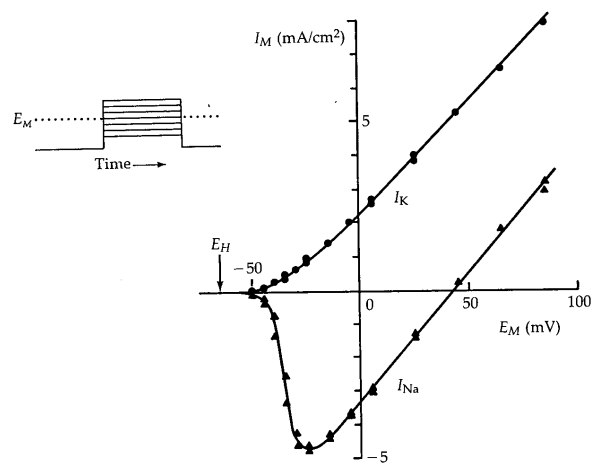


Figure 26: Relationship between current amplitude and membrane potential, taken from experiment such as in fig. 25. Whereas the late outward current increases steeply with increasing depolarization, the early inward current first increases in magnitude, but then decreases and reverses to outward current at about +50 mV [3].

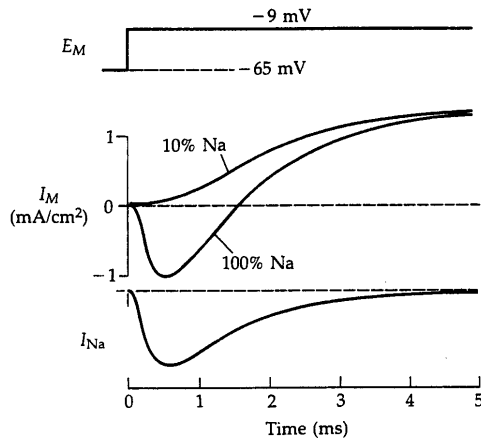


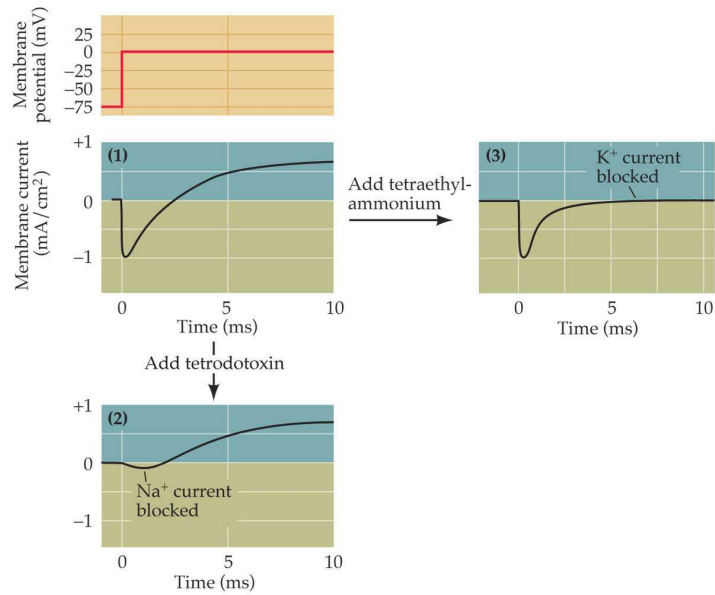
Figure 27: Dependence of the early inward current on sodium. In the presence of a normal external concentration of Na^+ , depolarization of a squid axon to -9 mV produces an inward initial current. However, reduction of the external Na^+ removes the early inward current. The external Na^+ concentration does not affect the late outward current [4].

An even more compelling way to test whether Na^+ carries the early inward current is to examine the behavior of this current after reducing the external Na^+ concentration by a factor of 10. In this case, both internal and external Na^+ concentrations are approximately equal and the Na^+ Nernst potential is close to 0 mV. In fig. 27, we see indeed that under this condition a voltage step to -9 mV does not evoke the early transient current, in agreement with the Na^+ hypothesis. Notice also that the reduction of external Na^+ has no effect on the outward current. This shows that the late outward current must be due to the flow of an ion other than Na^+ . Several lines of evidence presented by Hodgkin, Huxley and others showed that this late current is caused by K^+ exiting the neuron. Modern evidence that there are distinct mechanisms for Na^+ and K^+ come from pharmacological studies using drugs that specifically affect these two currents (fig. 28).

Hodgkin and Huxley used a simple relation between current and voltage such as eq. 8 to calculate the dependence of the conductance on voltage:

$$I_i = g_i(V, t)(V - V_i), \quad i = \text{K}^+, \text{Na}^+ \quad (9)$$

with V_i the reversal potential for ion i , V the membrane potential and I_i



NEUROSCIENCE, Third Edition, Figure 3.5 © 2004 Sinauer Associates, Inc.

Figure 28: Pharmacological separation of Na⁺ and K⁺ currents. Panel 1 shows the current that flows when the membrane potential of a squid axon is depolarized to -10 mV in control conditions. 2) Treatment with tetrodotoxin causes the early Na⁺ currents to disappear but spare the late K⁺ currents. 3) Addition of tetraethyl-ammonium blocks the K⁺ currents without affecting the Na⁺ currents [5, 6]

the ion current. Some examples of the current voltage relations are given in fig. 29. A and B show the passive case, where the conductance does not depend on voltage nor time, for different g_i and V_i . C and D show what shapes can occur when the conductance is voltage dependent but independent of time. Note the similarity in shape between figs. 29E and 26.

From fig. 26 and eq. 9 and from the known reversal potentials V_i one can compute the conductance $g_i(V)$ as a function of voltage. The result is shown in fig. 30. Hodgkin and Huxley concluded that both conductances are voltage dependent and increase sharply when the membrane is depolarized.

In addition, Hodgkin and Huxley showed that the conductances change over time. For example, both Na^+ and K^+ conductances require some time to *activate*. In particular, the K^+ conductance has a pronounced delay, requiring several milliseconds to reach its maximum (see fig. 31). The more rapid activation of the Na^+ conductance allows the resulting inward Na^+ current to precede the delayed outward K^+ current. The Na^+ current quickly declines even though the membrane potential is kept at a depolarized level. This fact shows that depolarization not only causes the Na^+ conductance to activate, but also cause it to decrease over time, or *inactivate*. The K^+ conductance of the squid axon does not inactivate in this way. Thus, while Na^+ and K^+ both show time dependent activation, only the Na^+ conductance in-activates. The time course of the Na^+ and K^+ conductances are also voltage dependent, with the speed of both activation and inactivation increasing at more depolarized potentials.

4.3 The Hodgkin-Huxley model

Hodgkin and Huxley's goal was to account for ionic fluxes and permeability changes in terms of molecular mechanisms. However, after intensive consideration of different mechanisms, they reluctantly concluded that still more needed to be known before a unique mechanism could be proven. Instead, they determined an empirical kinetic description that would be sufficiently good to predict correctly the major features of excitability. This is called the Hodgkin Huxley (HH) model.

The HH model is given in fig. 32. It consists of the Na^+ and K^+ currents, a capacitative term and a leakage term. The Na^+ and K^+ currents are each described by eq. 9. These currents are zero when the membrane potential is equal to their respective reversal potentials $V_i, i = \text{Na}^+, \text{K}^+$. The conductances of these currents are both voltage and time dependent as we

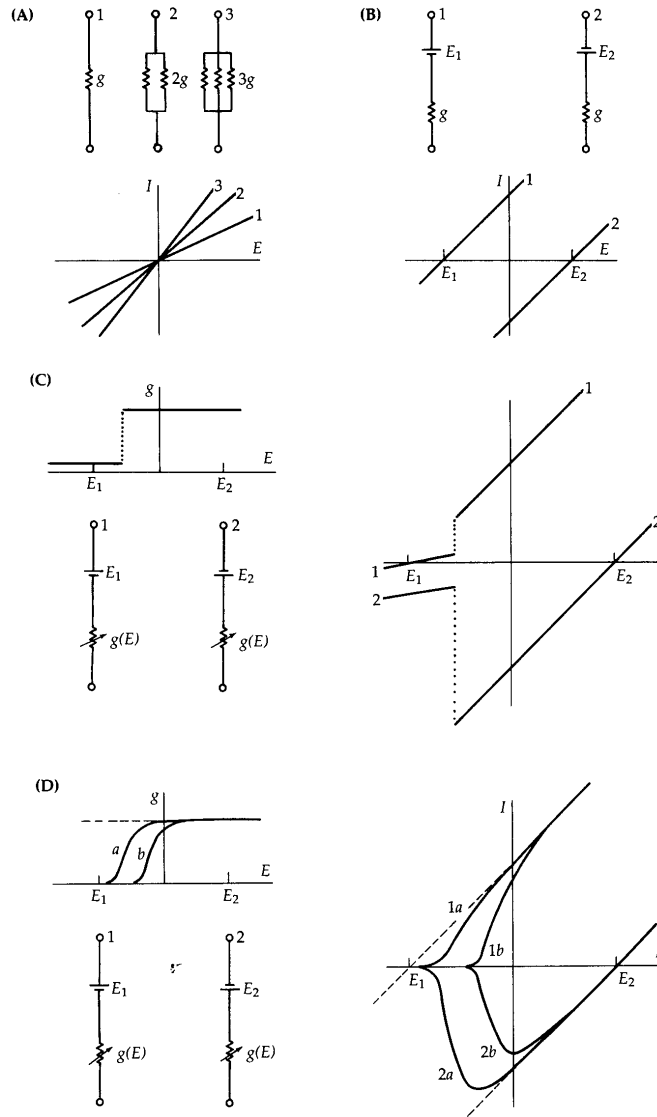


Figure 29: A) Conductance increases when more channels are open; B) Nernst or reversal potential differs for different ions or same ion in different bathing solutions; C-D) Conductance is voltage dependent.

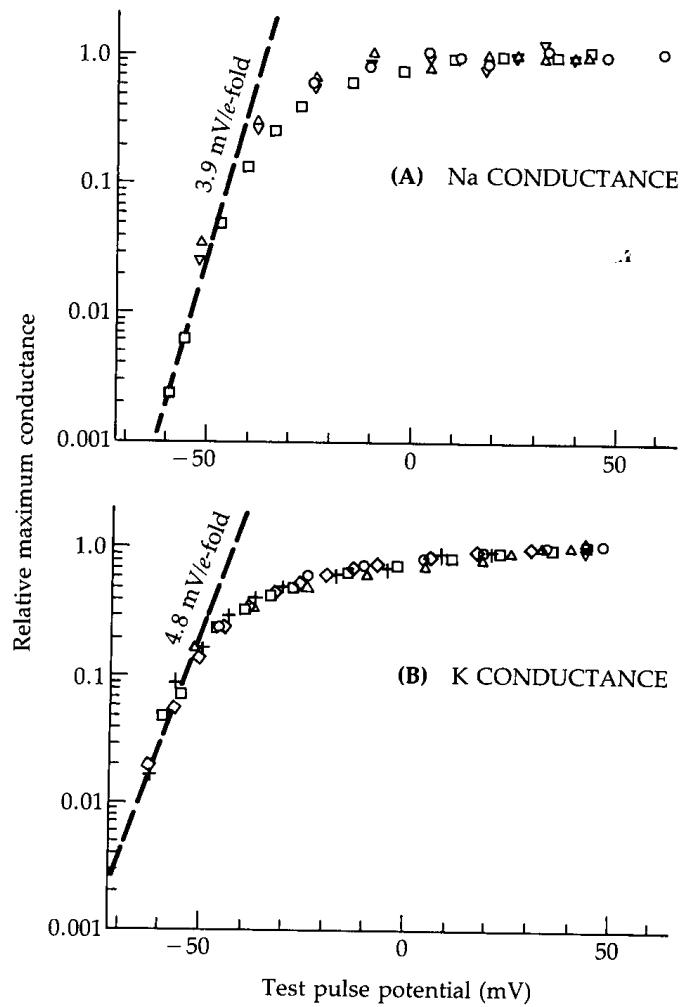


Figure 30: Depolarization increases Na^+ and K^+ conductances of the squid giant axon. The peak magnitude of Na^+ conductance and steady-state value of K^+ conductance both increase steeply as the membrane potential is depolarized [7].

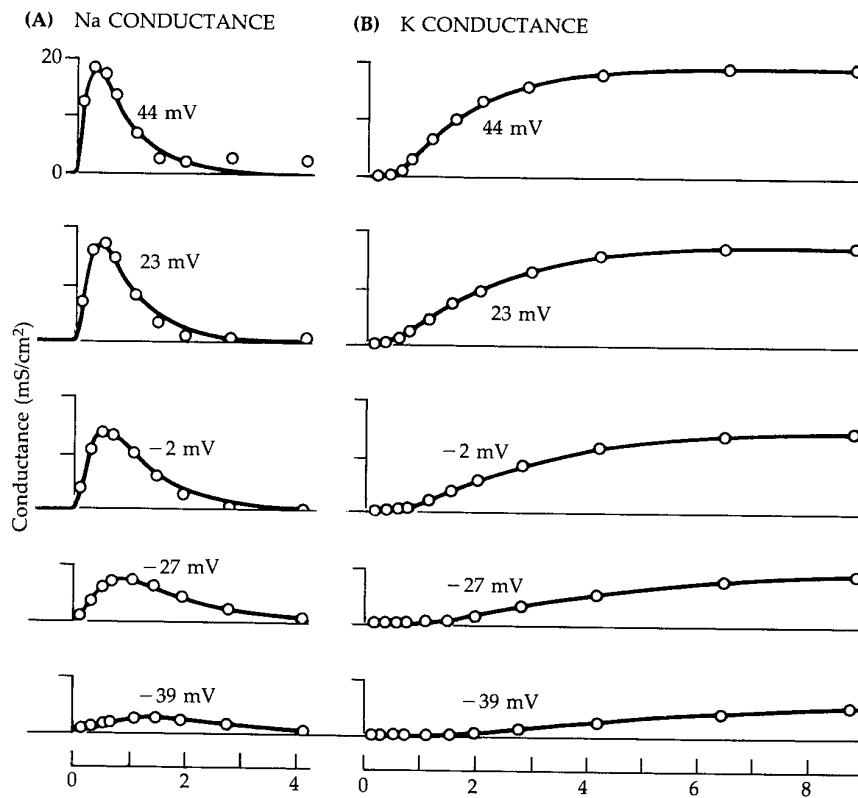


Figure 31: Membrane conductance changes underlying the action potential are time- and voltage-dependent. Both peak Na^+ and K^+ conductances increase as the membrane potential becomes more positive. In addition, the activation of both conductances occur more rapidly with larger depolarizations [7].

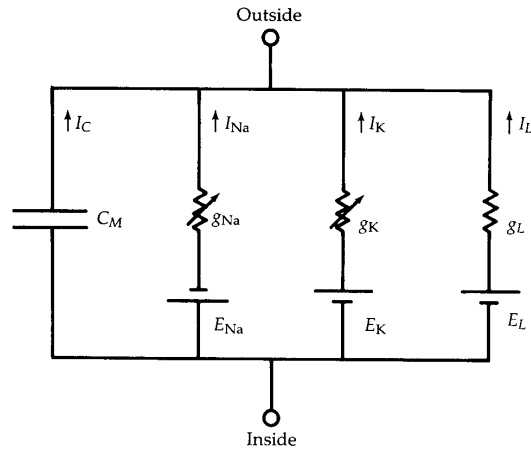


Figure 32: The Hodgkin Huxley model for the squid giant axon describes the membrane as an electrical circuit with four parallel branches.

will describe shortly.

The leakage term is of the similar form eq. 9 but with a passive conductance (time-independent and voltage independent). The leakage reversal potential is empirically determined to be close to 0 mV ¹

In addition, there is a capacitive branch. As we discuss in exercise 1, the concentration difference of the ions results in a charge build-up with opposite charge on either side of the membrane. To lowest order, the charge is proportional to the potential difference:

$$Q = CV$$

with Q the charge in Coulomb per unit area and C the capacitance. Because the membrane is so thin ($a \approx 2$ nm), we can safely treat the membrane as

¹The leakage conductance is the inverse of the resistance. The resistance is proportional to the thickness of the membrane. Also, the resistance of a sheet of membrane will decrease when we consider a larger area. Thus, we define the *resistivity* ρ as a property of the membrane material so that the resistance of a membrane of thickness a and area A is

$$R = \frac{\rho a}{A}.$$

two parallel planes, separated by a distance a . Then the capacitance is given by

$$C = \frac{\epsilon\epsilon_0 A}{d} \quad (10)$$

For hydrocarbon $\epsilon \approx 2$, this results in a very high specific capacitance of $\approx 1\mu F/\text{cm}^2$. The current through the capacitor is

$$I_c = C \frac{dV}{dt}, \quad (11)$$

where V is the membrane potential relative to the resting potential V_{rest} .

We will now model the time and voltage dependence of the K^+ and Na^+ currents. Because it is simpler, we first consider the K^+ conductance.

4.3.1 The K^+ conductance

The time and voltage dependence of g_{K^+} is empirically given in fig. 31. HH proposed to write the conductance as

$$g_{\text{K}^+} = \bar{g}_{\text{K}^+} n^4 \quad (12)$$

with \bar{g}_{K^+} the maximal conductance when all K^+ channels are open. n is a dynamic quantity and its differential equation is given by

$$\tau_n(V) \frac{dn}{dt} = n_\infty(V) - n \quad (13)$$

τ_n and n_∞ are the characteristic time constant for change in n and its stationary value, respectively. Both are voltage dependent (but time independent), as we see from fig. 31. The detailed dependence of τ_n and n_∞ on the membrane potential is given in fig. 33.

The response of eqs. 12 and 13 to a depolarizing voltage step is shown in fig. 34. It is seen, that the exponent 4 ensures that the K^+ conductance increases with slope zero in agreement with experiment. Instead, if g_{K^+} were proportional to n it would increase with non-zero slope. The exponent 4 was found at the time to give the best numerical fit. It was hypothesized by HH that the K^+ channel is controlled by four independent gates. All gates must be open for the channel to be open. If n denotes the probability that one of the gates is open, this reasoning explains the exponent 4 in eq. 12.

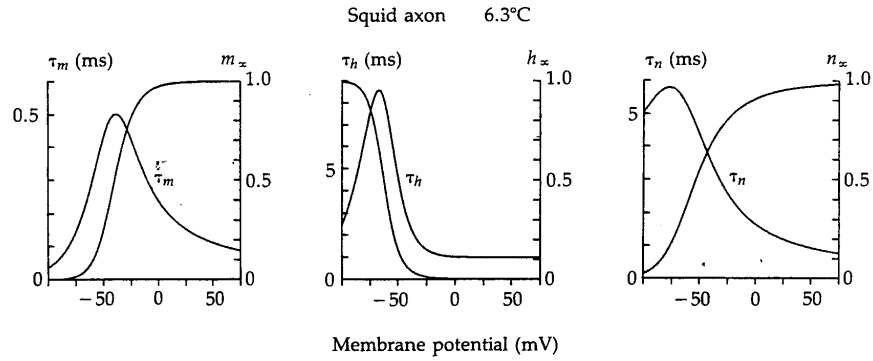


Figure 33: Dependence of the characteristic time constants $\tau_{m,h,n}$ and steady state values m_∞, h_∞ and n_∞ on the squid axon membrane potential. These values produce the solid lines in fig. 31.

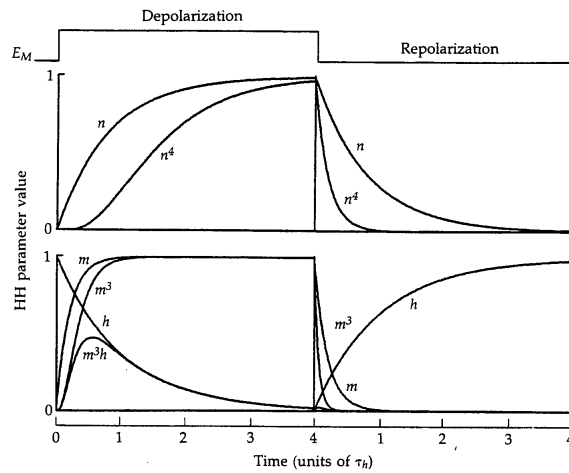


Figure 34: Response of n , h and m to a depolarizing and re-polarizing potential.

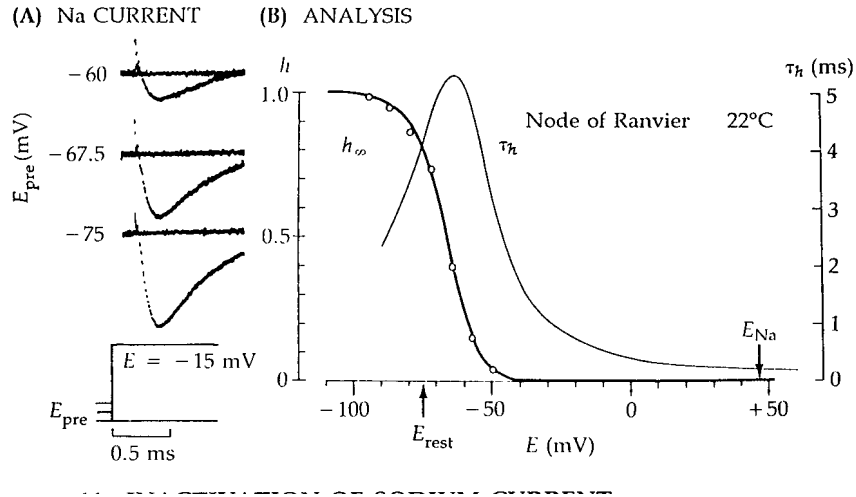


Figure 35: Inactivation of sodium current. A) Sodium currents elicited by test pulses to -15 mV after 50 milliseconds pre-pulses to three different levels. The current is decreased by depolarizing pre-pulses. B) The relative peak size of the sodium current versus the pre-pulse potential, forming the steady state inactivation curve of the HH model. Bell-shaped curve shows the voltage dependence of the exponential time constant of the inactivation process.

4.3.2 The Na^+ conductance

The Na^+ conductance is more complicated than the K^+ conductance, because there are independent activation and inactivation processes at work. The effect of Na^+ inactivation is shown in fig. 35. In this experiment, the dependence of the Na^+ current on the resting potential before the voltage step is shown. The membrane potential is first clamped to -60 , -67.5 or -75 mV for 50 milliseconds. Subsequently, the membrane potential is raised to -15 mV. The figure shows that the peak value of the resulting Na^+ current decreases with increasing pre-step membrane potential. The explanation of this phenomenon is the Na^+ inactivation. As a result of the pre-step clamping, the voltage dependent Na^+ inactivation will settle to different values. The equilibrium inactivation $1 - h_\infty$ is an increasing function of the membrane potential: For hyper-polarized membrane potential, inactivation is zero ($h_\infty = 1$) and activation of the channel yields the largest current. For a par-

tially depolarized membrane potential, the inactivation settles to a non-zero value and thus $h_\infty < 1$.

Hodgkin and Huxley postulated that the Na^+ conductance is given by

$$g_{\text{Na}^+} = \bar{g}_{\text{Na}^+} m^3 h \quad (14)$$

with \bar{g}_{Na^+} the maximal conductance when all Na^+ channels are open. m and h are dynamic quantities similar to n . Their differential equation is given by

$$\tau_m(V) \frac{dm}{dt} = m_\infty(V) - m \quad (15)$$

$$\tau_h(V) \frac{dh}{dt} = h_\infty(V) - h \quad (16)$$

$\tau_{m,h}$ are the characteristic time constants for change in m and h , respectively. m_∞ and h_∞ are their stationary values. All are voltage dependent, as we see from fig. 33.

For the resting membrane, the activation variable m_∞ and the inactivation variable $1 - h_\infty$ are close to zero. During a spike, m increases from zero to one, while h decreases from 1 to zero. As a result, the product $m^3 h$ shows a peak with a shape similar to the early transient Na^+ current (fig. 34).

4.3.3 Action potentials

We can now summarize the Hodgkin Huxley model. From fig. 32 we have

$$I_c + I_{\text{Na}^+} + I_{\text{K}^+} + I_{\text{leak}} + I_{\text{ext}} = 0$$

where we have added an external current, that we can use to provide current input to the cell. Combining eqs. 9-16, we obtain

$$\begin{aligned} C \frac{dV}{dt} &= -m^3 h \bar{g}_{\text{Na}^+} (V - V_{\text{Na}^+}) - n^4 \bar{g}_{\text{K}^+} (V - V_{\text{K}^+}) \\ &\quad - \bar{g}_{\text{leak}} (V - V_{\text{leak}}) - I_{\text{ext}}(t) \\ \tau_n \frac{dn}{dt} &= n_\infty - n \\ \tau_m \frac{dm}{dt} &= m_\infty - m \\ \tau_h \frac{dh}{dt} &= h_\infty - h \end{aligned} \quad (17)$$

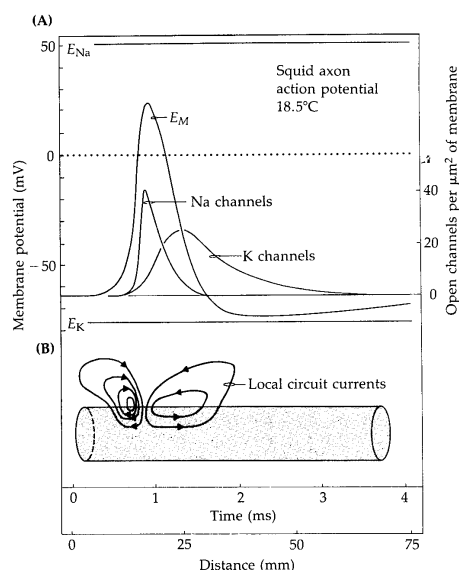


Figure 36: A) The solution of the Hodgkin-Huxley eqs. 17 for the membrane potential V and the conductances $\bar{g}_{K^+}n^4$ and $\bar{g}_{Na^+}m^3h$ as a function of time. Membrane depolarization rapidly opens Na^+ channels, causing an inrush of Na^+ ions, which in turn further depolarized the membrane potential. Slower inactivation of Na^+ and activation of K^+ channels restores the membrane potential to its resting value. B) Local current flows associated with propagation. Inward current at the excited region spreads forward inside the axon to bring the unexcited regions above the firing threshold.

where V_i and $\bar{g}_i, i = K^+, Na^+, leak$ are constants and $\tau_{n,m,h}$ and n_∞, m_∞ and h_∞ are voltage dependent as given in fig. 33. Thus, the HH equations constitute a coupled set of 4 non-linear first order differential equations.

The HH equations were developed to describe the voltage and time dependence of the K^+ and Na^+ conductances in a voltage clamp experiment. However, they can in fact also generate the form and time course of the action potential with remarkable accuracy (fig. 36). The initial depolarization of the membrane is due to the stimulus. This increases the Na^+ permeability, which yields a large inward Na^+ current, further depolarizing the membrane, which approaches the the Na^+ Nernst potential V_{Na^+} . The rate of depolarization subsequently falls both because the electrochemical driving force on

Na^+ decreases and because the Na^+ conductance in-activates. At the same time, depolarization slowly activates the K^+ conductance, causing K^+ ions to leave the cell and re-polarizing the membrane potential toward V_{K^+} . Because the K^+ conductance becomes temporarily higher than it is in the resting condition, the membrane potential actually becomes briefly more negative than the normal resting potential (the undershoot). The hyper-polarization of the membrane potential causes the voltage-dependent K^+ conductance (and any Na^+ conductance not in-activated) to turn off, allowing the membrane potential to return to its resting level.

4.4 Spike propagation

The voltage dependent mechanisms of action potential generation also explains the long-distance transmission of these electrical signals. This transmission forms the basis of information processing between neurons in the brain. Table 37 shows some conduction velocities for different types of nerve fibers. As we see, thick axons and myelinated fibers conduct much faster than thin and unmyelinated fibers, as we will explain below. Spike propagation is an active process, more like burning a fuse than electrical signaling in a copper wire. The latter is impossible because the axon longitudinal resistance is exceedingly high due to its small diameter. Therefore, one needs repeated amplification along the axon, which is what the spikes do. However, we first discuss passive current flow.

4.4.1 Passive current flow

Current conduction by wires, and by neurons in the absence of action potentials, is called passive current flow. It plays a central role in action potential propagation, synaptic transmission and all other forms of electrical signaling in nerve cells. For the case of a cylindrical axon, such as the one depicted in Fig. 38, subthreshold current injected into one part of the axon spreads passively along the axon until the current is dissipated by leakage out across the axon membrane.

Radial currents (through the membrane) as well as axial currents (along the axon axis) result from ion movement, which is due to the electric field as well as due to diffusion. We assume that we can safely ignore the contribution due to diffusion, ie. Ohms law is valid (see discussion of the Nernst-Planck equation in section 3.4). The axial current is much larger than the radial

Table 1. Conduction Velocities in Nerve and Muscle

<i>Tissue</i>	<i>Temperature</i> °C	<i>Myelinated (M)</i> <i>or</i> <i>unmyelinated (U)</i>	<i>Fibre</i> <i>Diameter</i> μ	<i>Velocity</i> m/sec.	<i>Notes</i>
Cat myelinated nerve fibres	38	M	2-20	10-100	a
Cat unmyelinated nerve fibres	38	U	0.3-1.3	0.7-2.3	a
Frog myelinated nerve fibres	24	M	3-16	6-32	b
Prawn myelinated nerve fibres	20	M	35	20	c
Crab large nerve fibres	20	U	30	5	d
Squid giant axon	20	U	500	25	d
Frog muscle fibre	20	U	60	1.6	d

(a) References, particularly Hursh (1939) in Patton (1960).

(b) Tasaki (1953).

(c) Holmes, Pumphrey & Young (1942).

(d) References and data in Katz (1948).

For myelinated fibres the figure given is the external diameter of the myelin.

Figure 37: Neural information processing depends on spike propagation from one cell to the next. The action potential lasts about 1 μ sec and travels at 1-100 m/sec.

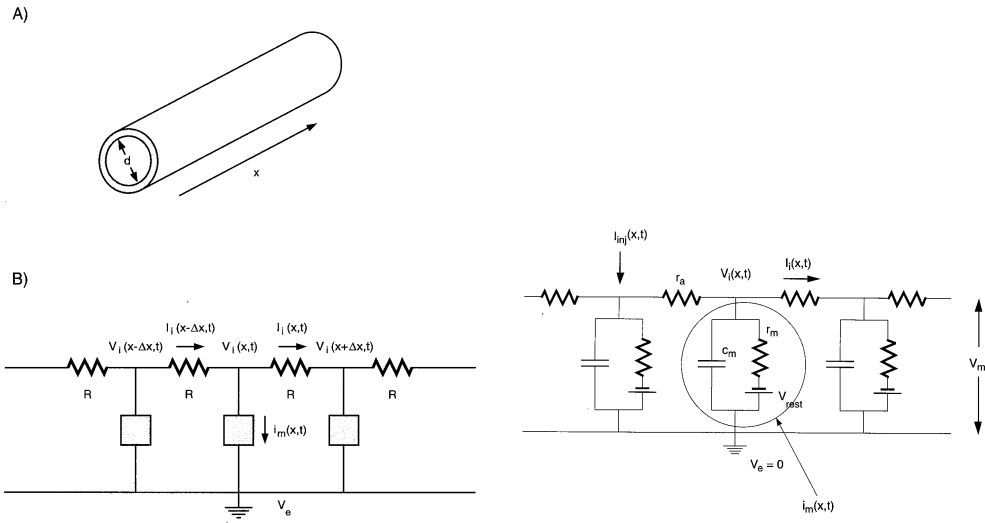


Figure 38: Linear cable model models the passive electrical properties of the axon.

current due to the fact that the membrane resistance is much higher than the intracellular resistance. Due to the small extracellular resistance, the external potential differences are small. Therefore, we assume a constant external potential independent of space and time.

As we will derive in exercise 5, the membrane potential, axial and radial membrane currents satisfies the following partial differential equations, known as the cable equation²:

$$\begin{aligned}
 \lambda^2 \frac{\partial^2 V}{\partial x^2} &= \tau_m \frac{\partial V}{\partial t} + V - r_m i_{inj} \\
 \frac{\partial V}{\partial x}(x, t) &= -r_a I_i(x, t) \\
 i_m(x, t) &= -\frac{\partial I_i}{\partial x}(x, t)
 \end{aligned} \tag{18}$$

with $V = V_i - V_{rest}$ the internal membrane potential with respect to the membrane resting potential; I_i is the axial current; $r_a \Delta x$ is the axial resistance of a cylinder of length Δx ; $i_m(x, t) \Delta x$ is the radial membrane current through

²These equations played an important role in the early 20th century for computing the transmission properties of transatlantic telephone cables.

a ring of thickness Δx ; $r_m/\Delta x$ is its resistance and $c_m\Delta x$ is its capacitance. $\lambda^2 = r_m/r_a$ and $\tau_m = r_m c_m$ the space and time constants.

Suppose, a constant current is injected at $x = 0$. The membrane potential reaches the steady-state solution satisfying

$$\begin{aligned}\lambda^2 \frac{d^2 V(x)}{dx^2} &= V(x) - r_m i_{\text{inj}}(x) \\ i_{\text{inj}}(x) &= I_0 \delta(x)\end{aligned}$$

The solution is given by

$$V(x) = V_0 \exp(-|x|/\lambda)$$

We can compute V_0 by observing that $\frac{dV}{dx} \Big|_{x=0} = -\frac{V_0}{\lambda} = -r_a I_i(x=0) = \frac{r_a I_0}{2}$ or

$$V_0 = \frac{r_a I_0 \lambda}{2} = \frac{\sqrt{r_a r_m}}{2} I_0$$

The membrane potential decreases with distance following a simple exponential decay, with characteristic length scale $\lambda = \sqrt{r_m/r_a}$. Hence, to improve the passive flow of current along an axon, the resistance of the membrane should be as high as possible and the resistance of the axoplasm should be low.

Due to the membrane capacitance, there is a time delay of the membrane potential response to a change in the input current. As a simplest example, consider the case that the potential is independent of location. If at $t = 0$ the injected current is changed from zero to a constant value I , the voltage response is easily computed from eq. 18:

$$V(t) = V_\infty (1 - \exp(-t/\tau_m))$$

with $V_\infty = I r_m$. We see that $V(t)$ changes with the characteristic time constant $\tau_m = r_m c_m$. In general, with more complex geometries than the cylindrical axon and a membrane potential that changes with x , the time course of the change in membrane potential is not simply exponential, but nonetheless depends on the membrane time constant.

We can easily get a rough idea of the conduction velocity in the passive cable as a function of the axon diameter d . First note, that since $r_m/\Delta x$ is the resistance through a ring of diameter d in radial direction, $r_m \propto d^{-1}$.

Secondly, since $r_a \Delta x$ is the resistance through a ring of diameter d in axial direction, $r_a \propto d^{-2}$. Thus, the characteristic length scale λ depends on the diameter as

$$\lambda = \sqrt{\frac{r_m}{r_a}} \propto \sqrt{d}$$

The capacitance of the ring is $c_m \Delta x$. Approximating the membrane as two parallel plates, the capacitance is proportional to the area of the ring: $c_m \propto d$. Thus, the characteristic time scale τ_m depends on the diameter as

$$\tau_m = r_m c_m \propto d^{-1} d = \text{constant}$$

We therefore estimate that the propagation velocity depends on the diameter of the axon as

$$v \propto \sqrt{d} \tag{19}$$

This requires very thick axons for fast propagation (eg. squid giant axon). From the examples of unmyelinated axons from table 37 we see indeed that they approximately follow this square root law. Fig. 39 summarizes the passive properties of the axon.

4.4.2 Spike propagation

If the experiment shown in Fig. 39 is repeated with a depolarizing current pulse sufficiently large to produce an action potential, the result is dramatically different (Fig. 40). In this case, an action potential occurs without decrement along the entire length of the axon, which may be a distance of a meter or more. Thus, action potentials somehow circumvent the inherent leakiness of neurons.

How, then, do action potentials traverse great distances along such a poor passive conductor? This is easy to grasp now we know how action potentials are generated and how current passively flows along an axon (Fig. 41). A depolarizing stimulus (synaptic input in in vivo situations or injected current pulse in an experiment) locally depolarize the axon, thus opening the voltage sensitive Na^+ channels in that region. The opening of Na^+ channels causes an action potential at that site. Due to the potential difference between that site and neighboring sites, current will flow to neighboring sites (as in passive conductance). This passive flow depolarizes the membrane potential in the adjacent region of the axon thus triggering an action potential in this region, and so forth. It is the active process of spike generation that boosts the

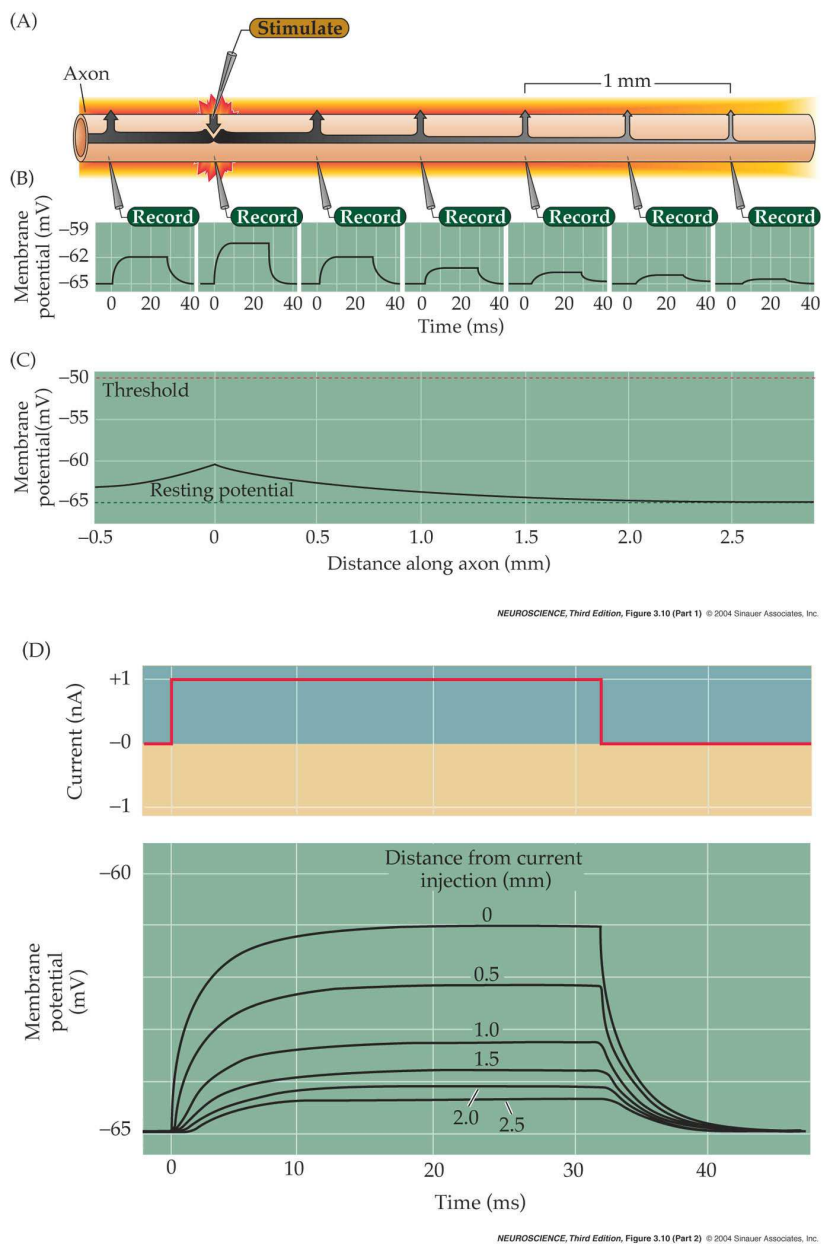
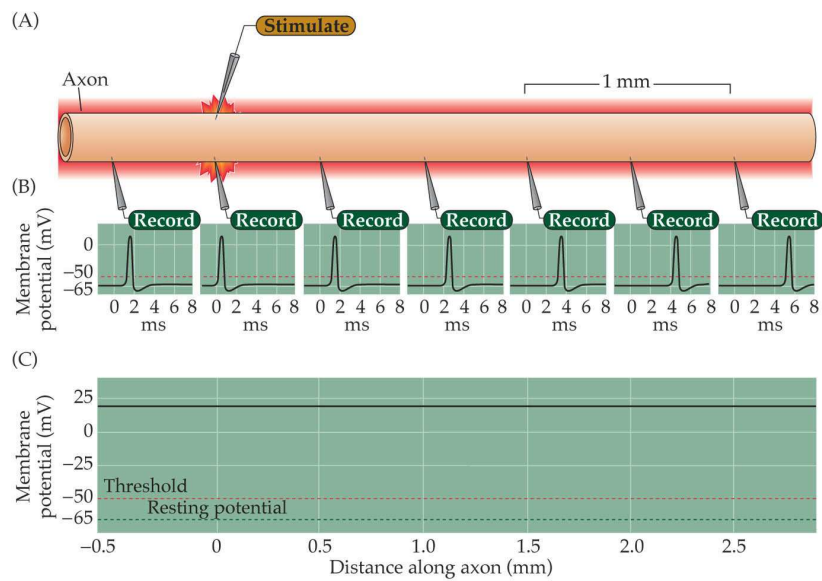


Figure 39: Passive current flow in an axon. A current passing electrode produces a subthreshold change in membrane potential, which spreads passively along the axon. With increasing distance from the site of current injection, the amplitude of the potential change is attenuated.



NEUROSCIENCE, Third Edition, Figure 3.11 © 2004 Sinauer Associates, Inc.

Figure 40: Propagation of an action potential. An electrode evokes an action potential by injecting a supra-threshold current. Potential response recorded at the positions indicated by micro-electrodes is not attenuated, but delayed in time.

signal at each site, thus ensuring the long-distance transmission of electrical signals.

After the action potential has passed a site, the Na^+ channels are inactivated and the K^+ channels are activated for a brief time (the refractory period) during which no spike can be generated. The refractoriness of the membrane in the wake of the action potential explains why action potentials do not propagate back toward the point of their initiation as they travel along an axon.

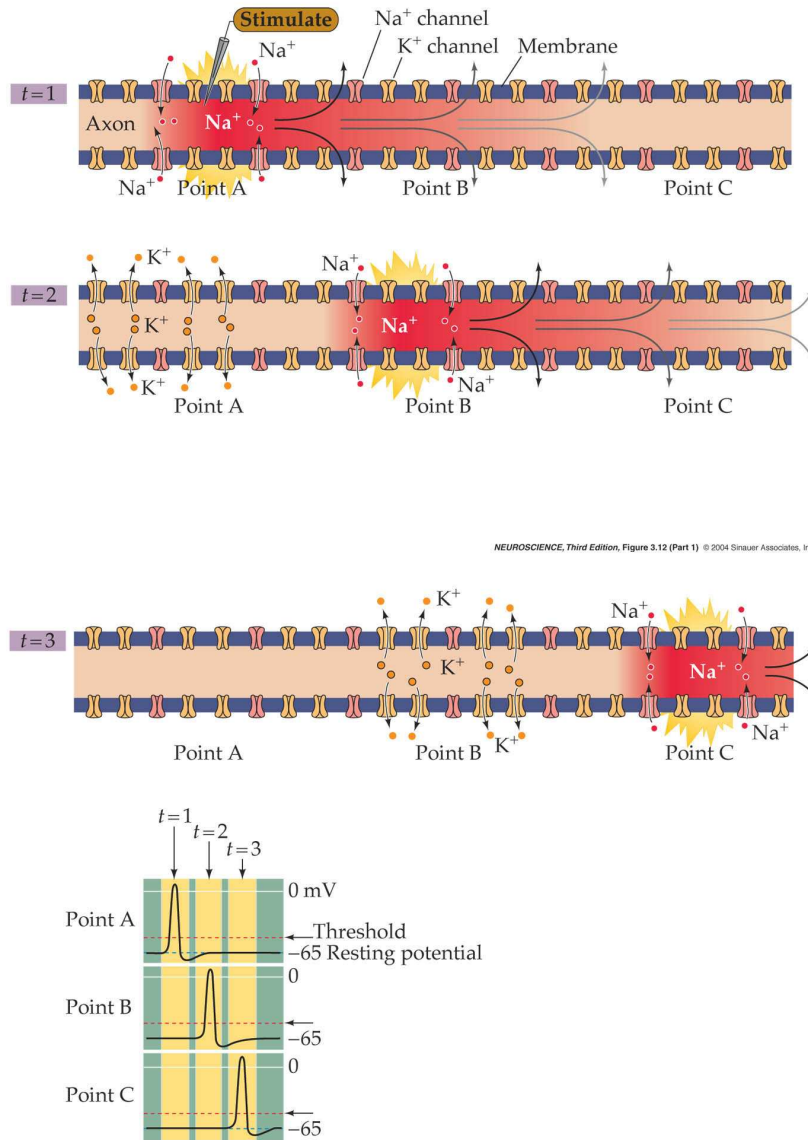
4.4.3 Myelin

Fast information processing in the nervous system require fast propagation of action potentials. Because action potential propagation requires passive and active flow of current, the rate of action potential propagation is determined by both of these phenomena. One way of improving passive current flow is to increase the diameter of the axon as we saw in section 4.4.1. However, this requires very thick axons for fast conduction.

Another strategy to improve the passive flow is to insulate the axonal membrane. For this reason, nerve fibers in vertebrates, except the smallest, are surrounded by a sheath of fatty material, known as myelin. The myelin sheath is interrupted at regular intervals, known as the nodes of Ranvier (Fig. 42). At these sites only, action potentials are generated. (If the entire surface of the axon were insulated, there would be no place for action potential generation.) An action potential generated at one node of Ranvier elicits current that flows passively within the myelinated segment until the next node is reached. The local current then generates an action potential in the next node of Ranvier and the cycle is repeated. Because action potentials are only generated at the nodes of Ranvier this type of propagation is called saltatory, meaning that the action potential jumps from node to node. As a result, the propagation speed of action potentials is greatly enhanced (Fig. 43).

This results in a marked increase in speed due to the increased speed of the passive conduction (see Exercise 6) and the time-consuming process of action potential generation occurs only at the nodes of Ranvier. Whereas unmyelinated axon conduction velocities range from about 0.5 to 10 m/s, myelinated axons can conduct at velocities up to 150 m/s.

Not surprisingly, loss of myelin, as occurs in disease such as multiple sclerosis, causes a variety of serious neurological problems.



NEUROSCIENCE, Third Edition, Figure 3.12 (Part 1) © 2004 Sinauer Associates, Inc.

NEUROSCIENCE, Third Edition, Figure 3.12 (Part 2) © 2004 Sinauer Associates, Inc.

Figure 41: Action potential conduction requires both active and passive current flow. Depolarization at one point along an axon opens Na^+ channels locally (Point 1) and produces an action potential at this point (A) of the axon (time point $t=1$). The resulting inward current flows passively along the axon (2), depolarizing the adjacent region (Point B) of the axon. At a later time ($t=2$), the depolarization of the adjacent membrane has opened Na^+ channels at point B, resulting in the initiation of the action potential at this site and additional inward current that again spreads passively to an adjacent point (Point C) farther along the axon (3). This cycle continues along the full length of the axon (5). Note that as the action potential spreads, the membrane potential re-polarizes due to K^+ channel opening and Na^+ channel inactivation, leaving a "wake" of refractoriness behind the action potential that prevents its backward propagation (4).

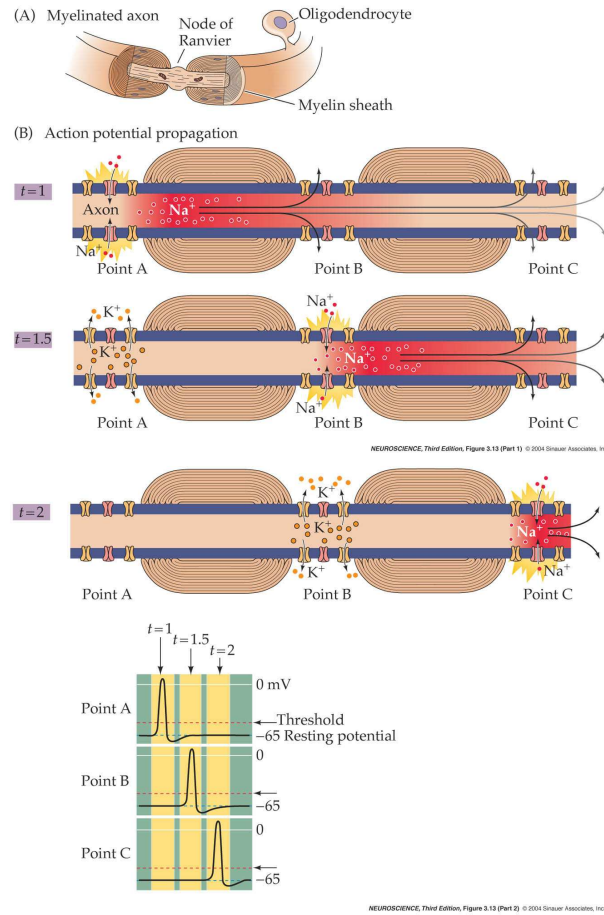


Figure 42: A) Diagram of a myelinated axon. B) Local current in response to action potential initiation at a particular site flows locally, as described in Fig. 41. However, the presence of myelin prevents the local current from leaking across the internodal membrane; it therefore flows farther along the axon than it would in the absence of myelin. Moreover, voltage-gated Na^+ channels are present only at the nodes of Ranvier. This arrangement means that the generation of active Na^+ currents need only occur at these unmyelinated regions. The result is a greatly enhanced velocity of action potential conduction. Bottom) Time course of membrane potential changes at the points indicated.

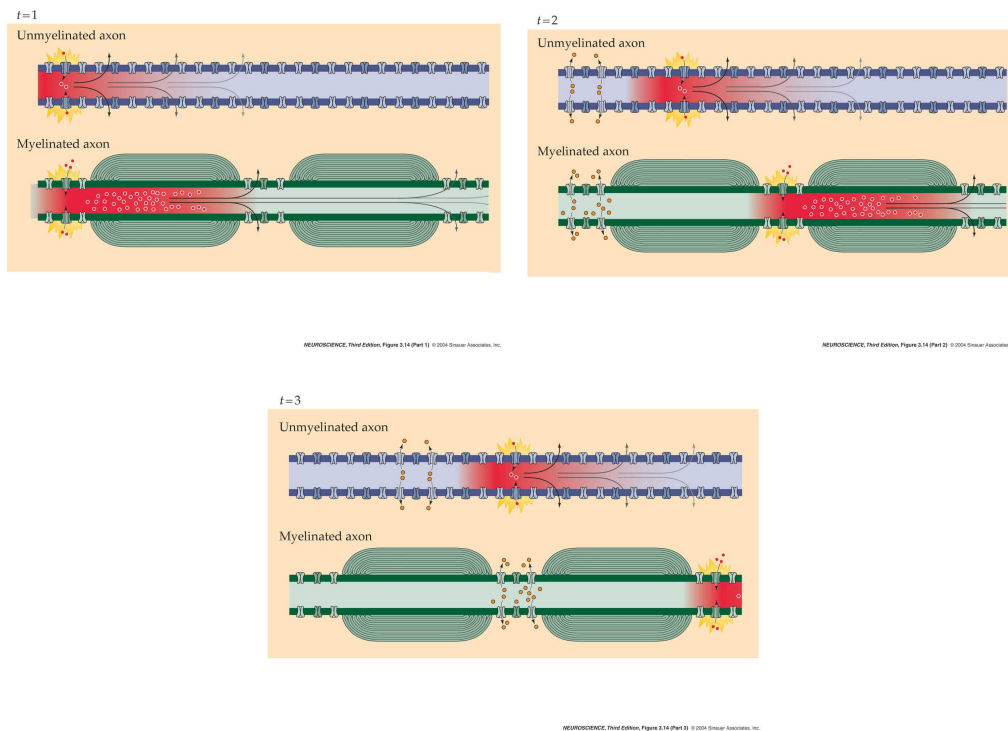


Figure 43: Comparison of speed of action potential conduction in unmyelinated (upper) and myelinated (lower) axons.

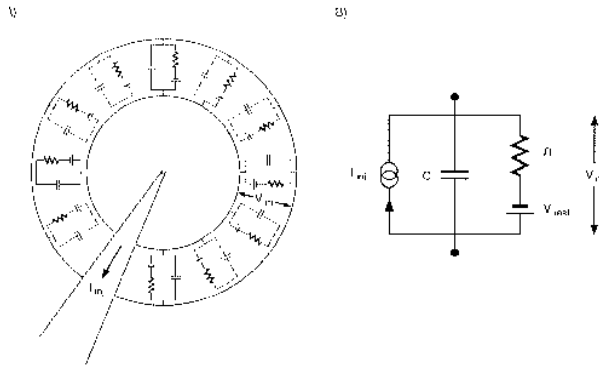


Figure 44: Equivalent electrical model of a nerve cell. The rest membrane potential is represented by a battery V_{rest} . The resistance $R = 1/G$, with G the linearized approximation Eq. 7. The capacitance is given by Eq. 10.

4.5 Summary

Contemporary understanding of membrane permeability is based on evidence obtained by the voltage clamp technique, which permits detailed characterization of permeability changes as a function of membrane potential and time. For most types of axons, these changes consist of a rapid and transient rise in the sodium permeability, followed by a slower but more sustained rise in the potassium permeability. Both permeabilities are voltage-dependent, increasing as the membrane potential depolarizes. The kinetics and voltage dependence of Na^+ and K^+ permeabilities provide a complete explanation of action potential generation. A mathematical model that describes the behavior of these permeabilities predicts virtually all of the observed properties of action potentials. The discussion of the voltage clamp method and the identification of the K^+ and Na^+ currents is based on [1] and the original papers [4, 7]. The discussion of the Hodgkin-Huxley model is based on [8].

4.6 Exercises

1. Passive properties of the nerve cell. If we ignore the spike generation mechanism of the nerve cell, we can describe the electrical behavior by an equivalent linear electronic circuit, as shown in fig. 44. The current through the resistor is equal to $I_r = V/R$ and the current through the

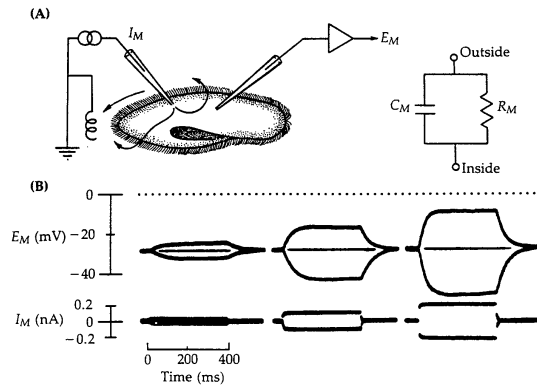


Figure 45: An experiment showing the passive electrical properties of a cell. The cell is impaled with two intracellular electrodes. One of them passes steps of current. The other records the changes of membrane potential.

capacitance is given by $C \frac{dV}{dt}$, with the capacitance is given by Eq. 10. In addition, there may be an externally supplied current I_{ext} .

Conservation of current implies

$$0 = I_c + I_r - I_{\text{ext}} = C \frac{dV}{dt} + \frac{V}{R} - I_{\text{ext}} \quad \tau \frac{dV}{dt} = -V + I_{\text{ext}} R$$

with $\tau = RC$ the membrane time constant.

In the cell in fig. 45 one measures the voltage change as a function of the amount of injected current. Assume that the cell can be described as an RC circuit

- (a) At $t < 0$ the membrane potential is at rest and the current $I(t) = 0$. Derive an expression for the membrane potential as a function of time if for $t > 0$ the current has a constant value $I_{\text{ext}}(t) = I_0$.
 - (b) Estimate approximately from fig. 45 the resistance of the cell and the RC time. Use these estimates to compute the surface area of the cell (assume the capacitance $C = 1 \mu F/cm^2$).
2. Consider the voltage clamp experiment in fig. 24. How would the current response be if the membrane permeability were not voltage dependent? Sketch the current response in fig. 24A and B.

3. Numerical simulation of the HH model in Matlab. For an introduction to Matlab see http://www.mines.utah.edu/gg_computer_seminar/matlab/matlab.html?. Download the software of numerical simulation of the HH model from www.snn.kun.nl/~bert/biofysica/fcns/spikes.zip. Unzip the file `spikes.zip` and go to the subdirectory `spikes`. The program `hh.m` simulates the Hodgkin-Huxley equations. In this program, $V - 60$ denotes the membrane potential in mV. The parameters α_i and β_i are related to the parameters $\tau_i, i = n, m, h$ and n_∞, m_∞ and h_∞ in Eq. 17 as

$$\begin{aligned}\tau_i &= \frac{1}{\alpha_i + \beta_i}, & i = n, m, h \\ n_\infty &= \alpha_n \tau_n \\ m_\infty &= \alpha_m \tau_m \\ h_\infty &= \alpha_h \tau_h\end{aligned}$$

The program `hh_functions.m` shows the dependence of these functions on membrane potential. By editing the program `hh.m`, we can study the behavior of the neuron as we change several parameters.

Study how the spiking of the neuron depends on the external current I_{ext} , by varying I_{ext} . Make a table of the spike frequency of the neuron versus the external current for $I_{ext} = 0, 5, 10, 40, 200 \mu A/cm^2$. What is the minimal value of the current for repetitive spiking? What happens to the frequency and amplitude for large current values?

4. In this exercise we compare the electrical resistance of an axon wire to a copper wire.
- Compute the resistance of one meter of axon if the axon resistivity $\rho = 100 \Omega cm$.
 - To how many meters of copper wire does this correspond if one meter of copper wire has a resistance of approximately 0.1Ω ?
5. Derive the cable equations 18 using Fig. 38.
6. Using a reasoning similar to that leading to eq. 19, derive an expression for the passive propagation velocity in myelinated axons as a function of the membrane thickness and axon diameter.

5 Synapses

5.1 Introduction

The human brain contains at least 100 billion neurons, each with the ability to influence many other cells. Clearly, highly sophisticated and efficient mechanisms are needed to enable communication among this astronomical number of elements. Such communication is made possible by synapses, the functional contacts between neurons. Although there are many kinds of synapses within the brain, they can be divided into two general classes: electrical synapses and chemical synapses. Electrical synapses permit direct, passive flow of electrical current from one neuron to another. The current flows through gap junctions, which are specialized membrane channels that connect the two cells. In contrast, chemical synapses enable cell-to-cell communication via the secretion of neurotransmitters: the chemicals released by the presynaptic neurons produce change the electrical conductance of the post-synaptic membrane by activating specific receptor molecules.

It is generally believed that the strength of chemical synapses can change through learning as a function of behavioral experience. Chemical synapses have therefore received most attention in the study of how networks of neurons can realize biological function. However, recently it has become clear that also electrical synapses may play an important role in neural information processing. In this chapter, however, we will restrict our attention to chemical synapses.

5.2 Chemical synapses

Chemical synapses come in a large variety and have a complex internal dynamics. Synapses typically connect the axon of one cell to the dendrite of another cell, but dendro-dendritic synapses also occur. Autapses, an axon making connection onto its own dendritic tree, are rare on pyramidal cells, but occur more frequently on some classes of cortical inhibitory inter-neurons.

Synapses are small: about 0.5-1.0 μm in diameter and are densely packed in the brain. If their size is 1 μm , one mm^3 full of synapses would contain 10^9 synapses. In fact, the experimental estimate is very close to this: 8×10^8 synapses/ mm^3 in mouse cortex. In addition, one mm^3 of brain tissue contains 100000 neurons, 4.1 **km** of axon ($d \approx 0.3\mu$) and 456 m of dendrite ($d \approx 0.9\mu$). Thus, the average neuron in the mouse cortex is connected to 8000 other

neurons and uses 4 mm of dendrite wire and 4 cm of axon wire to connect to other cells. Since the total cortical surface in humans is about 100000 mm² and 2 mm thick, there are about 2×10^{10} neurons and 2×10^{14} synapses in the human brain. Fig. 2 shows some examples of chemical synapses in adult cat visual cortex.

The space between the pre-and postsynaptic neurons is called the synaptic cleft. The key feature of all chemical synapses is the presence of small (30-40 nm diameter), membrane-bounded organelles called synaptic vesicles within the presynaptic terminal. These vesicles are filled with one or more neurotransmitters. These chemical agents act as messengers between the communicating neurons that gives this type of synapse its name.

Transmission at chemical synapses is based on an elaborate sequence of events (Fig. 46). 1) Action potential causes an inrush of Ca^{2+} ions via voltage dependent Ca channels. 2) Elevated Ca^{2+} concentration allows one or more vesicles to fuse with the presynaptic neuron membrane, releasing its neurotransmitter. 3) The neurotransmitter binds to postsynaptic receptors, increasing the permeability of post-synaptic ion channels. An in- or out-rush of current temporarily changes the post-synaptic potential (PSP).

5.3 The post-synaptic potential

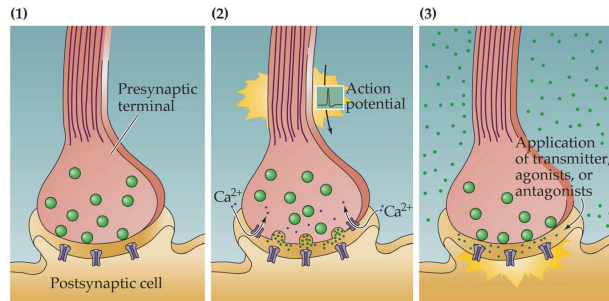
Upon activation of a chemical synapse one can observe a rapid and transient change in the postsynaptic potential. The response can be either excitatory (EPSP) or inhibitory (IPSP). These EPSPs and IPSPs are caused by excitatory and inhibitory post-synaptic currents (EPSCs and IPSCs).

The synaptic current rises fast and decays to zero in 20-30 msec. We see from Fig. 47 that the peak can be either positive or negative, depending on the clamping potential. The peak current is linearly related to the membrane potential. This suggest that:

$$I_{\text{syn}}(t) = g_{\text{syn}}(t)(V_m - V_{\text{syn}})$$

The post-synaptic current is caused by a temporary increase in the membrane conductance, modeled by $g_{\text{syn}}(t)$. V_{syn} is the clamp voltage for which the response changes sign. Its value is synapse specific.

Electrical properties of a membrane with synapse can be very simply described by an RC circuit as depicted in Fig. 48. Conservation of current



NEUROSCIENCE, Third Edition, Chapter 5, Box A © 2004 Sinauer Associates, Inc.

Figure 46: Canonical chemical synapse model. Action potential causes an inrush of Ca^{2+} ions via voltage dependent Ca channels. 2) Elevated Ca^{2+} concentration allows one or more vesicles to fuse with the presynaptic neuron membrane, releasing its neurotransmitter. 3) The neurotransmitter binds to postsynaptic receptors, increasing the permeability of post-synaptic ion channels. An in- or out-rush of current temporarily changes the post-synaptic potential (PSP).

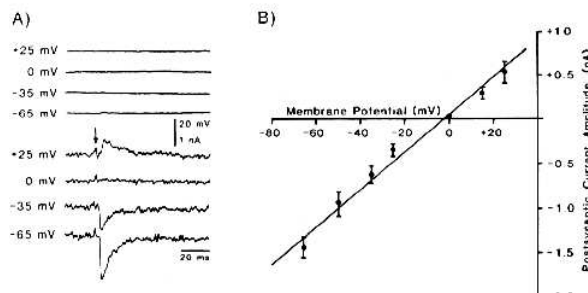


Figure 47: Activation of synapses made by the mossy fibers onto CA3 pyramidal cells in the rodent hippocampus. A) The pyramidal cell is voltage clamped to different values and the clamp current is recorded. B) Plot of Postsynaptic Current Amplitude (nA) versus Membrane Potential (mV) showing a linear relationship.

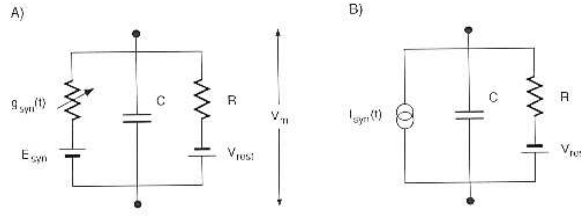


Figure 48: Equivalent electrical circuit for fast voltage dependent chemical synapse.

gives

$$C \frac{dV_m}{dt} + g_{\text{syn}}(t)(V_m - V_{\text{syn}}) + \frac{V_m - V_{\text{rest}}}{R} = 0$$

$$\tau \frac{dV}{dt} = -(1 + Rg_{\text{syn}})V - Rg_{\text{syn}}(V_{\text{rest}} - V_{\text{syn}})$$

with $V = V_m - V_{\text{rest}}$ and $\tau = RC$.

When $V_{\text{syn}} > V_{\text{rest}}$ the current will depolarize the membrane. An example is the excitatory synapse using the neurotransmitter glutamate with $V_{\text{syn}} - V_{\text{rest}} = 80\text{mV}$. When $V_{\text{syn}} < V_{\text{rest}}$ the current will hyper-polarize the membrane. An example is the inhibitory synapse using the neurotransmitter GABA_B that lets K ions out of the cell with $V_{\text{syn}} - V_{\text{rest}} = -10\text{--}30\text{mV}$. The situation is illustrated in Fig. 49

Shunting inhibition occurs when $V_{\text{rest}} = V_{\text{syn}}$. There is no synaptic current, but such synapses reduce the effect of other synapses. Consider one shunting synapse and one excitatory synapse:

$$\tau \frac{dV}{dt} = -(1 + Rg_{\text{syn}} + Rg_{\text{sh}})V - Rg_{\text{syn}}(V_{\text{rest}} - V_{\text{syn}})$$

The term Rg_{sh} reduces the peak response of V . An example is the GABA_A synapse that increases the conductance to Cl ions with a reversal potential near the resting potential of many cells.

The summation of EPSPs and IPSPs by a postsynaptic neuron permits a neuron to integrate the electrical information provided by all the inhibitory and excitatory synapses acting on it at any moment. If the sum of all input results in a depolarization of sufficient amplitude to raise the membrane potential above threshold, then the postsynaptic cell will produce an action potential (Fig. 50).

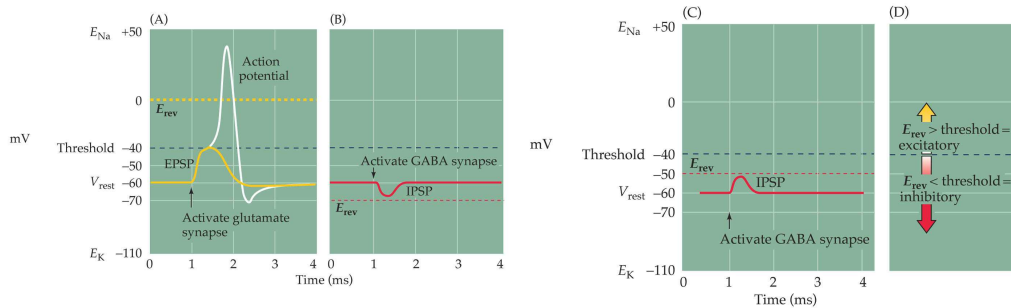


Figure 49: Reversal potentials and threshold potentials determine postsynaptic excitation and inhibition. A, C) If the reversal potential for a PSP (E_{rev}) is more positive than the action potential threshold (-40 mV), the effect of a transmitter is excitatory, and it generates an EPSP. B) If the reversal potential for a PSP is more negative than the action potential threshold, the transmitter is inhibitory and generates IPSPs.

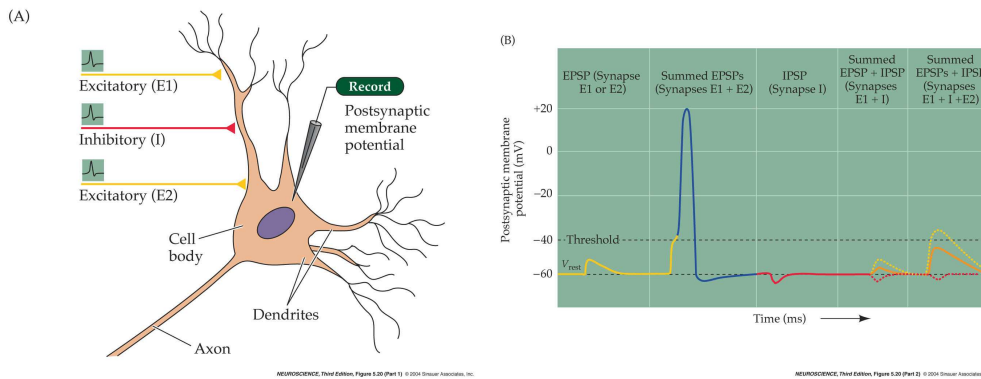


Figure 50: Summation of postsynaptic potentials

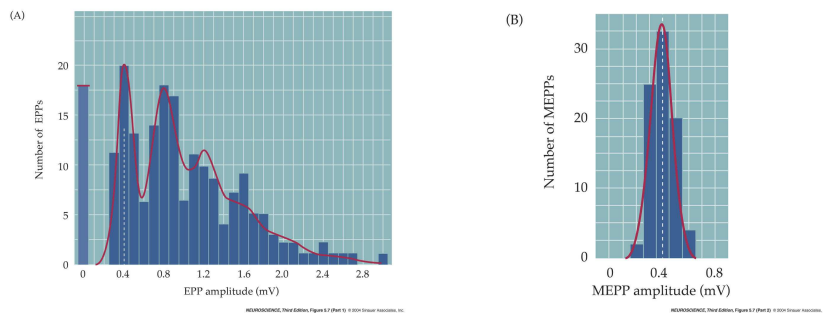


Figure 51: Histogram of 198 miniature EPSPs after presynaptic stimulation and 78 spontaneous EPSPs (inset).

5.4 Stochastic PSPs

Much of the evidence leading to the present understanding of chemical synaptic transmission was obtained from experiments at the neuromuscular junction. These synapses between spinal motor neurons and skeletal muscle cells are simple, large, and peripherally located, making them particularly amenable to experimental analysis [9].

Stimulation of the presynaptic motor neuron under normal conditions leads to a post synaptic action potential and contraction of the muscle. However, also in the absence of stimulation, one can observe post-synaptic EPSPs, so-called miniature EPSPs, that are the result of spontaneous neurotransmitter release. Measuring the size of these events shows that they are always more or less of the same magnitude (Fig. 51 inset). This suggests that these EPSPs are the result of the release of a single vesicle of neurotransmitter.

To test this hypothesis, Katz measured the post synaptic potential resulting from presynaptic stimulation when the concentration of Ca^{2+} in the extracellular medium is strongly reduced. In that case, the post-synaptic cell does not generate an action potential and a sub-threshold post synaptic response is observed instead. The magnitude of the response differs from trial to trial and the response is displayed as a histogram in Fig. 51. It is seen that the responses are clustered around multiples of 0.4 mV, which is the mean size of the spontaneous ('quantal') release mentioned above. Thus, pre-synaptic stimulation can lead to the opening of zero, one, two or up to five vesicles of neurotransmitter. On average $m = 2.33$ vesicles are released.

We can model this process by assuming that the junction has n release

k	$np(k)$	Observed
0	19	18
1	44	44
2	52	55
3	40	36
4	24	25
5	11	12
6	5	5
7	2	2
8	1	1
9	0	0

Table 3: Numerical comparison between observed quantal response of synapse in neuro-muscular junction and prediction from binomial distribution. $n = 198, m = 2.33$.

sites (n is a few hundred for neuro-muscular junction), each having an independent probability p of releasing a vesicle after pre-synaptic stimulation. p depends of course on the Ca^{2+} concentration. The probability that the synapse releases k quanta is then given by the binomial distribution

$$\begin{aligned}
 p(n, k) &= \binom{n}{k} p^k (1-p)^{n-k} \\
 m &= \langle k \rangle = np \\
 \sigma^2 &= \langle k^2 \rangle - m^2 = np(1-p)
 \end{aligned}$$

In the limit, $p \rightarrow 0, n \rightarrow \infty$ with $m = pn$ constant, the binomial distribution can be approximated by the Poisson distribution

$$p(n, k) \rightarrow p(k) = \frac{m^k}{k!} \exp(-m)$$

and the number of events for each k is given by $np(k)$. As is demonstrated in exercise 1, $np(k)$ reproduces these experimental findings very well.

With $m = 2.33$, the expected results for each k are compared with the experimentally observed results in Table 3 and we see that the agreement is excellent.

$m = 2.33 \ll n$ due to low external Ca. In normal operation $m = \mathcal{O}(n)$.

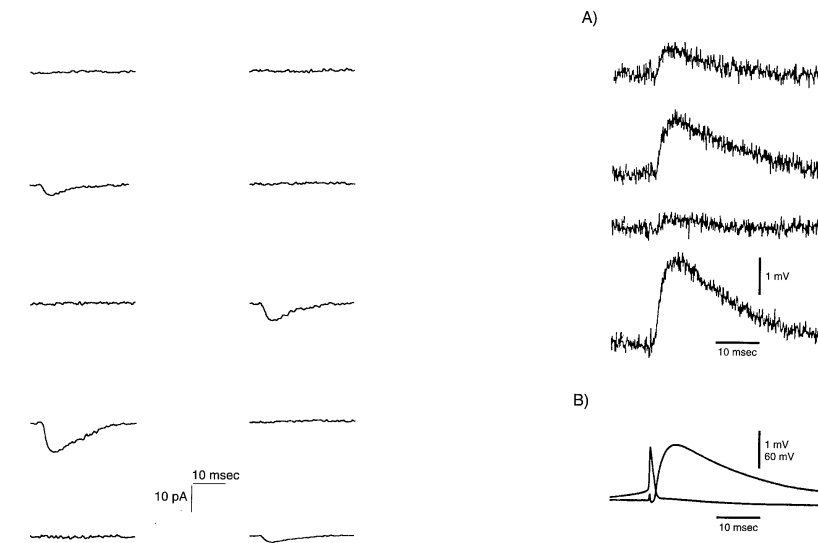


Figure 52: Left. EPSC in CA 1 pyramidal cells. Only 3 out of 9 presynaptic stimuli produce a response. In addition, the response is variable in strength. Right. Rat visual cortex. 4 EPSPs resulting from identical stimulation.

Whereas the neuro-muscular junction has many hundreds of synaptic contact, in cortex one finds mostly mono-synaptic connections and $0.1 < p < 0.9$. Thus, information transmission between individual neurons is noisy and unreliable, as is illustrated in fig. 52.

5.5 Learning

The earliest learning experiments are from the psychology literature. First there is the phenomenon of habituation using Pavlov's dog. In this experiment a bell rings (CS) and the dog turns her head (CR). After several repetitions, the dog stops paying attention to the bell. Thus, the same stimulus leads to a change in the response from 'head turn' to 'no head turn' (fig. 53b).

Depending on the type of stimulus, habituation occurs or not. If the dog is shown a piece of meat (US), the dog will salivate (UR). UR) on sight of meat (US). No matter how often the stimulus is presented, the dog will always respond (fig. 53c).

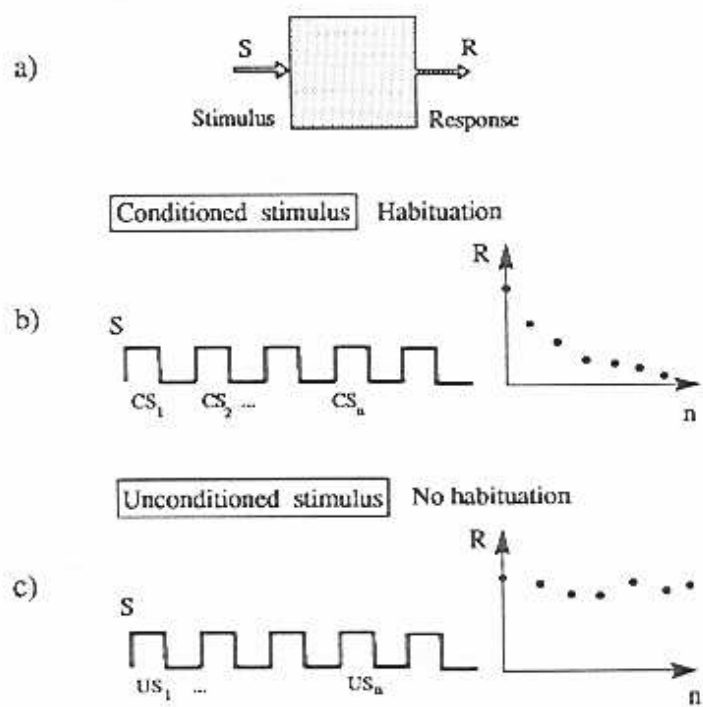
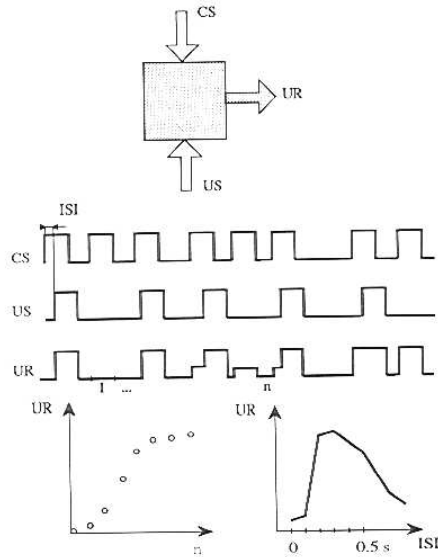


Figure 53: Habituation experiments

Now, consider two stimuli CS (bell) and US (meat). By itself CS does not yield a response, but US does. Classical conditioning is the phenomenon that when CS and US are presented together for some time, the dog will start responding to CS alone.



This phenomenon can be explained by assuming a simple model that captures the relation between stimuli and response:

$$R = \Theta(J^u S^u + J^c S^c - \theta)$$

$\Theta(x)$ is a threshold function that returns 1 for $x > 0$ and zero otherwise. $R = 1, 0$ denotes the response of the dog salivating or not, $u = 1, 0$ denotes the presence of the unconditioned stimulus (meat) and $c = 1, 0$ denotes the presence of the conditioned stimulus (bell). J_u and J_c are connections modulating the dependence of R on u and c , respectively. If this model is operational in the brain somewhere, J_u and J_c can be thought of as effective synaptic connections between neurons or groups of neurons.

Before the experiment the bell by itself does not yield a response, but the meat does. Therefore: $J^c < \theta$ and $J^u > \theta$. After the experiment both bell and meat yield the response. Therefore: $J^c > \theta$ and $J^u > \theta$. We can understand the change in J_c by the so-called Hebbian learning paradigm

$$\Delta J \propto RS$$

The synaptic strength J is only increased when the post-synaptic response R coincide with the pre-synaptic stimulus S . In the absence of the meat stimulus, the bell stimulus never yields a response $R = 1$ and therefore the connection J_c between bell and salivate is not strengthened. When both bell and meat are presented, the meat stimulus by itself will make the dog salivate ($R = 1$). The Hebbian learning rule will then strengthen both the connections J_c and J_u . When J_c grows in this way and exceeds θ , the dog will start salivating when only the bell is presented. The strengthening of J_u has no effect since its value is larger than θ from the beginning.

5.6 Long term potentiation

Many synapses in the mammalian central nervous system exhibit long-lasting forms of synaptic plasticity that are plausible substrates for learning, memory and permanent changes in behavior.

One experimentally observed pattern of synaptic activity is known as long-term potentiation (LTP). LTP has been studied most in the hippocampus, an area of the brain that is especially important in the formation and/or retrieval of some forms of memory.

The progress in understanding LTP has relied heavily on in vitro studies of slices of living hippocampus. The hippocampus contains several regions, the major ones being CA1 and CA3. Much of the work on LTP has focused on the synaptic connections between the Schaffer collaterals (axons of CA3 pyramidal cells) and CA1 pyramidal cells. The experimental setup is illustrated in Fig. 54. A stimulus electrode can activate a Schaffer collateral. Single stimuli applied to a Schaffer collateral evokes EPSPs in the post-synaptic CA1 neuron. These stimuli alone do not elicit any change in synaptic strength. However, when the CA1 neuron's membrane potential is briefly depolarized (by applying current pulses through the recording electrode) in conjunction with the Schaffer collateral stimuli, there is a persistent increase in the EPSPs, which can last for hours or days. LTP occurs not only at the excitatory synapses of the hippocampus, but at many other synapses in a variety of brain regions, including the cortex, amygdala and cerebellum.

LTP is a specific strengthening of synaptic connection, without strengthening other synapses that contact the same neuron (Fig. 55A). Another important property is associativity (Fig. 55B). As noted, weak stimulation of a pathway will not by itself trigger LTP. However, if one pathway is weakly activated at the same time that a neighboring pathway onto the same cell is

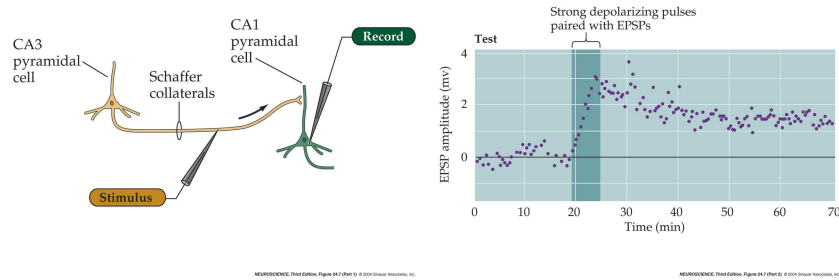


Figure 54: Pairing presynaptic and postsynaptic activity causes LTP.

strongly activated, both synaptic pathways undergo LTP. Note, that this is a cellular analog of the previously discussed mechanism for classical conditioning.

5.7 Hebbian learning

The simplest plasticity rule that follows the spirit of Hebb's conjecture takes the form

$$\tau_w \frac{dw}{dt} = vu - \lambda v \quad (20)$$

where w is the synaptic strength, τ_w is a time constant that controls the rate at which the weights change, and u and v are the neural activity of the pre- and post-synaptic cell, respectively. The first term on the right hand side of Eq. 20 is the Hebbian term and increases the synapses proportional to the product of pre- and post-synaptic activity. Hebbian plasticity is a positive-feedback process because effective synapses are strengthened, making them even more effective. This tends to increase post-synaptic firing rates excessively.

The second term is an effective way of controlling this instability and decreases the synapse proportional to the total post-synaptic activity. λ is an adjustable constant. For one presynaptic neuron and one post-synaptic neuron the net effect is that the synapse is increased (decreased) when the pre-synaptic activity $u > \lambda$ ($u < \lambda$).

When u and v are changing with time, w will also change with time according to Eq. 20. A nice simplification can be made when we assume that

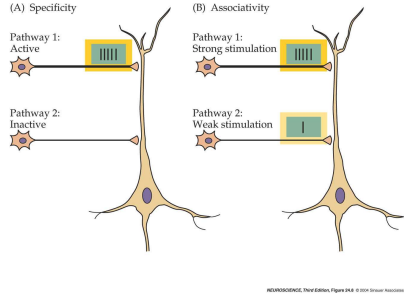


Figure 55: A) Strong activity initiates LTP at active synapses without initiating LTP at nearby inactive synapses. B) Weak stimulation of pathway 2 alone does not trigger LTP. However, when the same weak stimulus to pathway 2 is activated together with strong stimulation of pathway 1, both sets of synapses are strengthened.

u and v are randomly drawn from a probability distribution $p(u, v)$. In this case the average synaptic weight satisfies

$$\tau_w \frac{dw}{dt} = \langle uv \rangle - \lambda \langle v \rangle$$

with $\langle uv \rangle = \int dudvp(u, v)uv$ and $\langle v \rangle = \int dudvp(u, v)v$.

When a neuron receives input from n synapses with strength w_i , the deterministic rule becomes

$$\tau_w \frac{dw_i}{dt} = vu_i - \lambda v, \quad i = 1, \dots, n \quad (21)$$

Note, that the change of each synapse depends on the value of all other synapses through v . For instance, if we assume that v depends linearly on the inputs $v = \sum_{i=1}^n w_i u_i$.

5.7.1 Ocular dominance

Hebbian plasticity is often used to model the development and activity-dependent modification of neuronal selectivity to various aspects of a sensory input, for example the selectivity of visually responsive neurons to the orientation of a visual image. This typically requires competition between synapses, so that the neuron becomes unresponsive to some features while

growing more responsive to others. The above Hebbian rule Eq. 21 introduces such competition, as we will show now.

We consider the highly simplified case of a single layer 4 neuron that receives input from just two LGN neurons with activity $u_i, i = 1, 2$. Two synaptic weights $w_i, i = 1, 2$ describe the synaptic connection strengths of the LGN neurons with the cortical neuron. The output activity we assume simply linear:

$$v = \sum_{i=1}^2 w_i u_i \quad (22)$$

Thus, Eq. 21 becomes

$$\begin{aligned} \tau_w \frac{dw_i}{dt} &= \sum_j Q_{ij} w_j - \lambda(w_1 \langle u_1 \rangle + w_2 \langle u_2 \rangle) \\ Q_{ij} &= \langle u_i u_j \rangle \end{aligned} \quad (23)$$

Using the symmetry property that both eyes are equal, we can parameterize the matrix as $Q_{11} = Q_{22} = q_s$, $Q_{12} = Q_{21} = q_d$ and $\langle u_1 \rangle = \langle u_2 \rangle = \langle u \rangle$. We can solve Eq. 23 by changing to the basis of eigenvectors of Q . Stated differently, the dynamical equations for $w_1 + w_2$ and $w_1 - w_2$ decouple:

$$\tau_w \frac{d(w_1 + w_2)}{dt} = (q_s + q_d - 2\lambda \langle u \rangle)(w_1 + w_2) \quad (24)$$

$$\tau_w \frac{d(w_1 - w_2)}{dt} = (q_s - q_d)(w_1 - w_2) \quad (25)$$

For λ sufficiently large, the first equation will yield the asymptotic solution $w_1 + w_2 = 0$. Under normal circumstances, the cross correlation between eyes q_d is smaller than the autocorrelation q_s . Therefore, $q_s - q_d > 0$ and $w_1 - w_2$ will grow indefinitely. In reality, there will be non-linearities in the system (in Eq. 20 and Eq. 22) that will prevent this indefinite growth. The final solution is then

$$w_1 = -w_2 = w_\infty \quad (26)$$

with w_∞ a positive or negative value depending on the sign of the initial value $w_1(0) - w_2(0)$. For $w_\infty > 0$, the cortical neuron will be sensitive to eye 1 and insensitive to eye 2, and vice versa. Thus, we have shown that ocular dominance can be explained as a consequence of Hebbian learning.

5.8 Summary

There are chemical and electrical synapses. Chemical synapses are thought to be implied in learning. Synapses can be excitatory, inhibitory or shunting depending on the reversal potential of the synapse relative to the membrane resting potential. Synapses are stochastic elements: a presynaptic action potential yields a postsynaptic response with a certain probability. The most important mechanism for learning is called Hebbian learning. The strength of a synapse increases when pre- and postsynaptic cell fire at the same time. This is in agreement with the psychological phenomenon of classical conditioning and also found as a mechanism for synaptic plasticity in the brain. Hebbian learning can be used to explain the receptive field properties of many neurons, such as for instance ocular dominance. This chapter is based on [10, 1, 11].

5.9 Exercises

1. This exercise is about the quantal release of neurotransmitter at the neuro-muscular junction.
 - (a) Show that the binomial distribution reduces to the Poisson distribution in the limit $p \rightarrow 0, n \rightarrow \infty$ with $m = pn$ constant.
 - (b) Check the numerical agreement between the Poisson distribution and the experimental values
 - (c) Discuss the shape of the distribution when the Ca^{2+} is restored to its normal physiological value. Compute the mean and variance and explain why under these conditions the presynaptic spike gives a deterministic post-synaptic response.

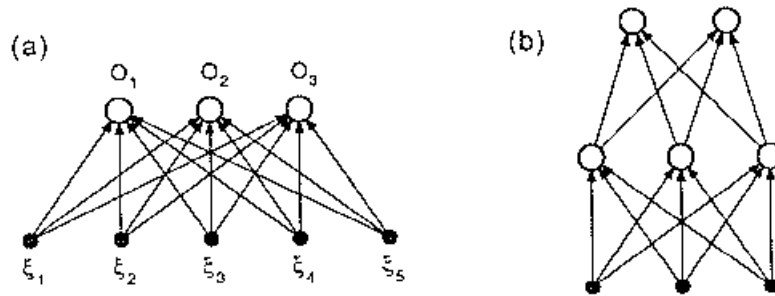


Figure 56: A) Simple Perceptron B) Multi-layered Perceptron

6 Perceptrons

Perceptrons are feed-forward neural networks. Examples are given in Fig. 56. Consider a simple perceptron with one output:

$$o = g(h) = g\left(\sum_{j=1}^n w_j \xi_j - \theta\right) = g\left(\sum_{j=0}^n w_j \xi_j\right)$$

with weights w_j and inputs ξ_j . $\xi_0 = -1$ and $\theta = w_0$. g is a non-linear function.

Learning: Given a number of input-output pairs $(\xi_j^\mu, \zeta^\mu), \mu = 1, \dots, P$, find w_j such that the perceptron output o for each input pattern ξ^μ is equal to the desired output ζ^μ :

$$o^\mu = g\left(\sum_{j=0}^n w_j \xi_j^\mu\right) = \zeta^\mu, \quad \mu = 1, \dots, P$$

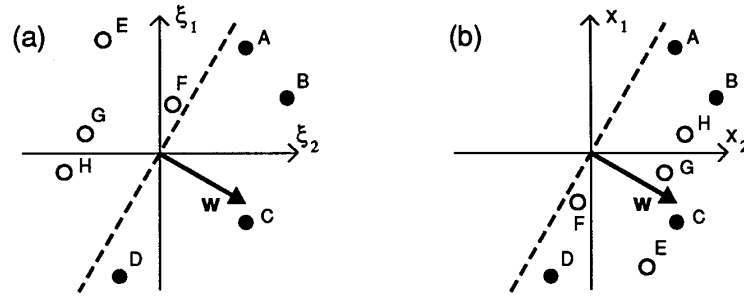
6.1 Threshold units

Consider the simplest case of binary threshold neurons:

$$g(h) = \text{sign}(h)$$

Then, the learning condition becomes

$$\text{sign}(w \cdot \xi^\mu) = \zeta^\mu, \quad \mu = 1, \dots, P$$



Since $\zeta^\mu = \pm 1$, we have

$$\text{sign}(w \cdot \xi^\mu \zeta^\mu) = 1 \quad \text{or} \quad w \cdot x^\mu > 0$$

with $x_j^\mu = \xi_j^\mu \zeta^\mu$.

6.2 Linear separation

Classification depends on sign of $w \cdot \xi$. Thus, decision boundary is hyper plane:

$$0 = w \cdot \xi = \sum_{j=1}^n w_j \xi_j - \theta$$

Perceptron can solve linearly separable problems. An example of a linearly separable problem is the AND problem: The output of the perceptron is 1 if all inputs are 1, and -1 otherwise (see Fig. 57).

By definition, problems that are not linearly separable need more than one separating hyper plane to separate the two classes. An example of a non-linearly separable problem is the XOR problem: The output is equal to the product of the input values (see Fig. 57A). Other problems that are not linearly separable occur when three or more input patterns are linearly dependent (see Fig. 57B).

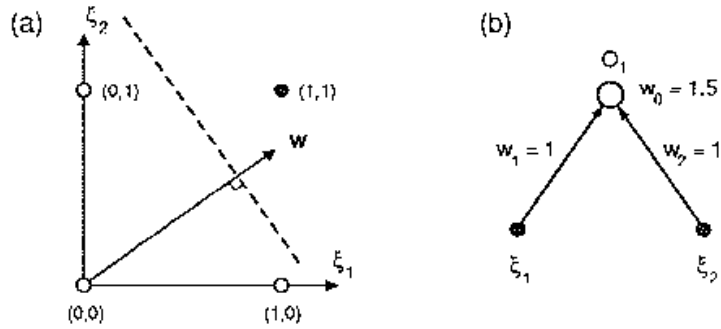
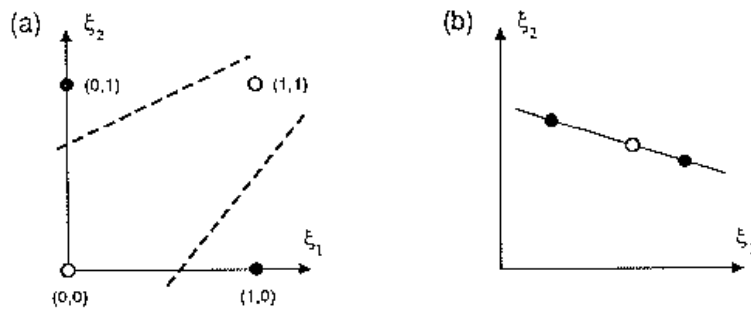


Figure 57: The AND problem for two inputs is linearly separable.



6.3 Perceptron learning rule

We have seen that the desired weight vector satisfies

$$w \cdot x^\mu > 0, \quad \text{all patterns} \quad (27)$$

We define the following perceptron learning rule:

$$\begin{aligned} w_j^{\text{new}} &= w_j^{\text{old}} + \Delta w_j \\ \Delta w_j &= \eta \Theta(-w \cdot x^\mu) \xi_j^\mu \zeta^\mu = \eta \Theta(-w \cdot x^\mu) x^\mu \end{aligned} \quad (28)$$

η is the learning rate. This learning rule is Hebbian in the sense that the change in weight is proportional to the product of input and output activity.

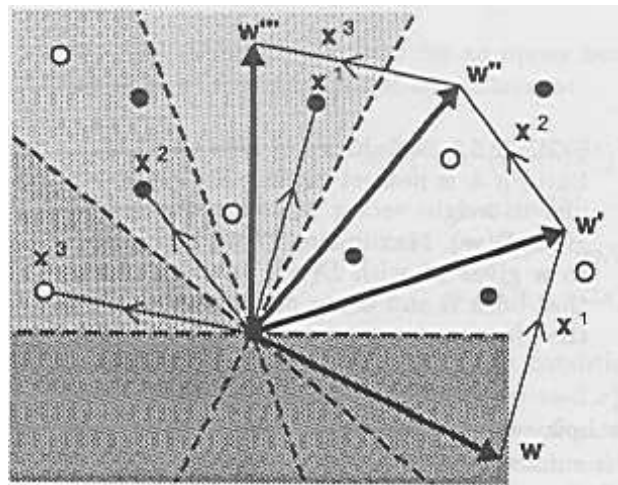


Figure 58: The perceptron learning rule in action. Learning rule Eq. 28 is applied to all patterns in some random or given order. Learning stops, when a weight configuration is found that has positive inner product with all training patterns.

The function Θ is 1 for positive arguments and zero otherwise: When presenting pattern μ , learning only occurs, when the condition $w \cdot x^\mu > 0$ is not satisfied for that pattern.

In Fig. 58 we show the behavior of the perceptron learning rule with $\eta = 1$. The dataset consists of three data patterns x^1, x^2 and x^3 . The initial weight vector is w . Presenting pattern x^1 , we note that $w \cdot x^1 < 0$ and therefore learning occurs. The resulting weight vector is $w' = w + x^1$. Presenting pattern x^2 and x^3 also result in learning steps and we end up in weight configuration w''' . This weight vector has positive inner product with all training patterns and learning terminates.

Depending on the data, there may be many or few solutions to the learning problem, or non at all! In Fig. 59 we give examples of two data sets and their solutions Eq. 27. In Fig. 59A there are more admissible weight vectors and they can have a larger inner product with all training patterns than in Fig. 59B. We define the quality of the solution w by the pattern that has the smallest inner product with w . Since the solution does not depend on the

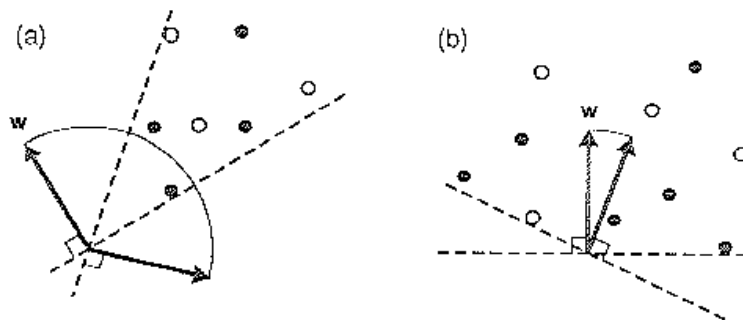


Figure 59: Two examples of data sets and the sets of w that satisfy condition Eq. 27. A) Many solutions B) Few solutions.

norm of w , we define the quality as

$$D(w) = \frac{1}{\|w\|} \min_{\mu} w \cdot x^{\mu}$$

The best solution is given by $D_{\max} = \max_w D(w)$.

In Fig. 60, we illustrate this for a given data set and two admissible solutions w and w' and their values of D respectively. Since $D(w') > D(w)$, w' is the preferred solution.

If we can find a w such that $D(w) > 0$ the problem is linearly separable and learnable by the perceptron learning rule. If the problem is not linearly separable not such solution exists.

6.3.1 Convergence of Perceptron rule

In this section we show that if the problem is linearly separable, the perceptron learning rule converges in a finite number of steps. We start with initial value $w = 0$. At each iteration, w is updated only if $w \cdot x^{\mu} < 0$. After some number of iterations, let M^{μ} denote the number of times pattern μ has been used to update w . Thus,

$$w = \eta \sum_{\mu} M^{\mu} x^{\mu}$$

$M = \sum_{\mu} M^{\mu}$ is the total number of iterations in which the weight vector is updated. If the learning rule converges, it means that M is finite and does not grow indefinitely.

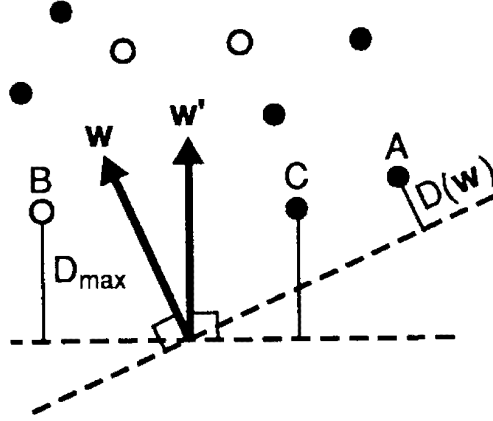


Figure 60: Two admissible solutions w and w' and their values of D respectively. Since $D(w') > D(w)$, w' is the preferred solution.

The proof goes as follows. Assume that the problem is linearly separable, so that there is a solution w^* with $D(w^*) > 0$. We will show that

$$\mathcal{O}(\sqrt{M}) \leq \frac{w \cdot w^*}{\|w\| \|w^*\|} \leq 1$$

where the second inequality follows simply from the definition of the inner product, and we will show the first inequality below. Thus, M can not grow indefinitely and the perceptron learning rule converges in a finite number of steps.

The proof of the first inequality is elementary:

$$\begin{aligned} w \cdot w^* &= \eta \sum_{\mu} M^{\mu} x^{\mu} \cdot w^* \geq \eta M \min_{\mu} x^{\mu} \cdot w^* = \eta M D(w^*) \|w^*\| \\ \Delta \|w\|^2 &= \|w + \eta x^{\mu}\|^2 - \|w\|^2 = 2\eta w \cdot x^{\mu} + \eta^2 \|x^{\mu}\|^2 \leq \eta^2 \|x^{\mu}\|^2 = \eta^2 N \end{aligned}$$

The inequality in the second line makes use of the fact that for each training pattern where learning takes place $w \cdot x^{\mu} < 0$. The norm of w is thus bounded by

$$\|w\|^2 \leq \eta^2 N M$$

Combining these two inequality, we obtain Thus,

$$\frac{w \cdot w^*}{|w||w^*|} \geq \sqrt{M} \frac{D(w^*)}{\sqrt{N}} \quad (29)$$

which completes the proof. Note, that the proof makes essential use of the existence of w^* with $D(w^*) > 0$. If $D(w^*) < 0$ the bound Eq. 29 becomes a trivial statement and does not yield a bound on M .

If the problem is linearly separable, we can in conclude that the number of weight updates:

$$M \leq \frac{N}{D^2(w^*)}$$

where N is some trivial constant. We see that convergence takes longer for harder problems (for which $D(w^*)$ is closer to zero).

6.4 Linear units

We now turn to a possibly simpler case of linear units:

$$o^\mu = \sum_j w_j \xi_j^\mu$$

Desired behavior is that the perceptron output equals the desired output for all patterns: $o^\mu = \zeta^\mu, \mu = 1, \dots, P$. In this case, we can compute an explicit solution for the weights. It is given by

$$w_j = \frac{1}{N} \sum_{\rho\nu} \zeta^\rho (Q^{-1})_{\rho\nu} \xi_j^\nu, \quad Q_{\rho\nu} = \frac{1}{N} \sum_j \xi_j^\rho \xi_j^\nu \quad (30)$$

Q is a matrix with dimension $P \times P$ and contains the inner products between the input patterns.

To verify that Eq. 30 solves the linear perceptron problem, we simply check for one of the input patterns (ξ^μ) whether it gives the desired output:

$$\begin{aligned} \sum_j w_j \xi_j^\mu &= \frac{1}{N} \sum_{\rho,u,j} \zeta^\rho (Q^{-1})_{\rho\nu} \xi_j^u \xi_j^\mu \\ &= \sum_{\rho,u} \zeta^\rho (Q^{-1})_{\rho\nu} Q_{\nu\mu} \\ &= \sum_{\rho} \zeta^\rho \delta_{\rho\mu} = \zeta^\mu \end{aligned}$$

For this solution to exist, Q must be invertible. Therefore, the input patterns must be linearly independent. Because otherwise Q is not of maximal rank. Therefore, the number of patterns cannot exceed the number of input dimensions: $P \leq N$.³

When $P < N$ the solution $w_j = \frac{1}{N} \sum_{\rho\nu} \zeta^\rho (Q^{-1})_{\rho\nu} \xi_j^\nu$ is not unique. In fact, there exists a linear space of dimension $N - P$ of solutions w . Namely, let

$$\begin{aligned} w_j^0 &= \frac{1}{N} \sum_{\rho\nu} \zeta^\rho (Q^{-1})_{\rho\nu} \xi_j^\nu \\ w_j &= w_j^0 + \xi^\perp \end{aligned}$$

with ξ^\perp an n -dimensional vector that is perpendicular to all training patterns: $\xi^\perp \perp \{\xi^\mu\}$. Then the output of the perceptron is unaffected by ξ^\perp :

$$\zeta^\mu = \sum_j w_j \xi_j^\mu = \sum_j (w_j^0 + \xi_j^\perp) \xi_j^\mu = \sum_j w_j^0 \xi_j^\mu$$

6.4.1 Gradient descent learning

Often $P > N$, and thus patterns are linearly dependent. In general, one can define a learning rules through a cost function, that assigns a cost or quality to each possible weight vector. A common cost function is the quadratic cost:

$$E(w) = \frac{1}{2} \sum_\mu \left(\zeta^\mu - \sum_j w_j \xi_j^\mu \right)^2$$

³If the input patterns are linearly dependent, solution Eq. 30 does not exist. Linear dependence of the inputs implies that there exists α^μ such that

$$\sum_\mu \alpha^\mu \xi_j^\mu = 0$$

This implies that

$$\sum_\mu \alpha^\mu \zeta^\mu = \sum_{\mu j} w_j \alpha^\mu \xi_j^\mu = 0$$

in other words, that the outputs cannot be chosen at freely. For problems with linearly dependent inputs and matched linearly dependent output Eq. 30 can be used by restricting the training set to a linearly independent subset that spans the training set, and computing Q for this subset.

which is minimized when the actual perceptron output $\sum_j w_j \xi_j^\mu$ is as close as possible to the desired output ζ^μ for all patterns μ .

The cost function can be minimized by the so-called gradient descent procedure. We start with an initial random value of the weight vector w and we compute the gradient in this point:

$$\frac{\partial E}{\partial w_i} = - \sum_{\mu} \left(\zeta^\mu - \sum_j w_j \xi_j^\mu \right) \xi_i^\mu$$

We change w according to the 'learning rule'

$$w_i = w_i + \Delta w_i \quad \Delta w_i = -\eta \frac{\partial E}{\partial w_i} \quad (31)$$

and repeat this until the weights do not change any more.

When η is sufficiently small, it is easy to verify that this gradient descent procedure converges. The proof consists of two observations. One is that for small η , $E(w)$ decreases in each step, and the other is that $E(w)$ is bounded from below, so that it has a smallest value. Therefore E cannot continue decreasing indefinitely and must converge to some stationary value (see Exercises).

6.4.2 The value of η

What is a good value for η ? Clearly, when η is very small, convergence is guaranteed, but in practice it may take a very long time. If η is too large, however, convergence is no longer guaranteed. The problem is further complicated by the fact that the optimal choice of η is different for different components of the weight vector w . This is illustrated in Fig. 61, where E as a function of w is drawn. This valley has a unique minimal value for E , but the curvature in two directions is very different. In the long (flat) direction, large steps can be made, but in the orthogonal direction only small steps are allowed. We can analyze the problem, by assuming that the energy has the form

$$E(w) = \frac{1}{2} \sum_i a_i (w_i - w_i^*)^2 + E_0$$

with w^* the location of the minimum, and a_i the curvatures in the two directions $i = 1, 2$. Eq. 31 becomes

$$\Delta w_i = -\eta \frac{\partial E}{\partial w_i} = -2\eta a_i (w_i - w_i^*) = -2\eta a_i \delta w_i$$

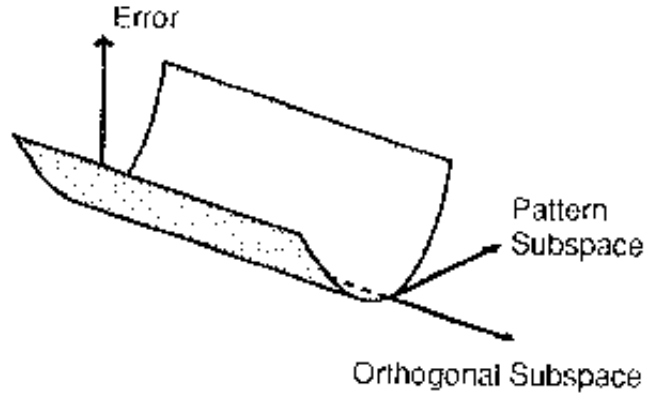


Figure 61: Cost landscape $E(w)$ with different curvatures in different directions.

with $\delta w_i = w_i - w_i^*$. The effect of learning step on δw_i is

$$\delta w_i^{\text{new}} = w_i^{\text{new}} - w_i^* = w_i^{\text{old}} - 2\eta a_i \delta w_i^{\text{old}} - w_i^* = (1 - 2\eta a_i) \delta w_i^{\text{old}}$$

thus, δw_i converges asymptotically to zero iff

$$|1 - 2\eta a_i| < 1. \quad (32)$$

We must find an η that satisfies Eq. 32 for all i . When $1 - 2\eta a_i < 0$, δw_i changes sign in each iteration. The behavior is illustrated in Fig. 62 with $E(w_1, w_2) = w_1^2 + 20w_2^2$ for different values of η .

6.5 Non-linear units

We can extend the gradient descent learning rule to the case that the neuron has a non-linear output:

$$o^\mu = g(h^\mu), \quad h^\mu = \sum_j w_j \xi_j^\mu$$

We use again the quadratic cost criterion:

$$E_1(w) = \frac{1}{2} \sum_\mu (\zeta^\mu - o^\mu)^2$$

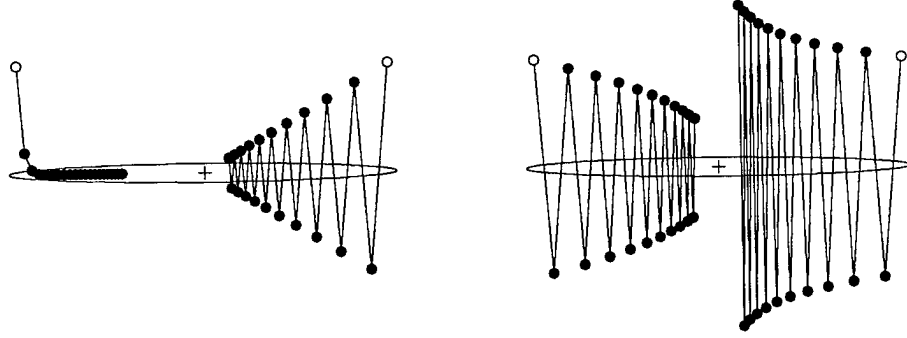


Figure 62: Behavior of the gradient descent learning rule Eq. 31 for the quadratic cost function $E(w_1, w_2) = w_1^2 + 20w_2^2$ for $\eta = 0.02, 0.0476, 0.049, 0.0505$.

$$\Delta w_i = -\eta \frac{\partial E}{\partial w_i} = \sum_{\mu} (\zeta^{\mu} - o^{\mu}) g'(h^{\mu}) \xi_i^{\mu}$$

When the function g is a monotonous function, it is invertible and one could also formulate a different cost criterion by observing the identity

$$\begin{aligned} \zeta^{\mu} &= g(h^{\mu}) \Leftrightarrow g^{-1}(\zeta^{\mu}) = h^{\mu} \\ E_2(w) &= \frac{1}{2} \sum_{\mu} \left(g^{-1}(\zeta^{\mu}) - h^{\mu} \right)^2 \end{aligned}$$

Note, that E_2 has a quadratic dependence on w , as in the linear case (but with transformed targets $g^{-1}(\zeta^{\mu})$ instead of ζ^{μ}). In general, optimizing either E_1 or E_2 yield different optimal solutions.

6.6 Multi-layered perceptrons

The gradient descent learning procedure can be trivially extended to the perceptron with multiple layers and multiple outputs as shown in Fig. 56B. In addition to the input variables ξ_k and the output variable o_i , we have a layer of hidden variables v_j for which no training data are observed. The

value of the hidden variables is computed in terms of the input variables, and the outputs are computed in terms of the hidden variables:

$$o_i = g\left(\sum_j w_{ij}v_j\right) = g\left(\sum_j w_{ij}g\left(\sum_k w_{jk}\xi_k\right)\right) \quad (33)$$

The output is now a complex function of the input pattern ξ_k and the weights w_{jk} in the first layer of the network and the weights w_{ij} in the second layer of the network.

Given a set of P training patterns $(\xi_k^\mu, \zeta_i^\mu), \mu = 1, \dots, P$, we again use the gradient descent procedure to find the weights that minimize the total quadratic error:

$$E(w) = \frac{1}{2} \sum_i \sum_\mu (o_i^\mu - \zeta_i^\mu)^2 \quad (34)$$

with o_i^μ the output on node i for input pattern ξ^μ as given by Eq. 33.

For large neural networks with many hidden units, the simple gradient descent procedure can be quite slow. However, there exist well-known algorithms that significantly accelerate the convergence of the gradient descent procedure. One such method is the conjugate gradient method. Treatment of this method is beyond the scope of this course (see however [12] or Matlab for further details).

Note, that the optimal solution that is found depends on the number of hidden units in the network. The more hidden units, the more complex functions between input and output can be learned. So, for a given data set, we can make the error Eq. 34 as small as we like by increasing the number of hidden units. In fact, one can show that the multi-layered perceptron can learn any smooth function, given a sufficiently large number of hidden units.

However, the objective of a learning algorithm is to use the neural network to predict the output on novel data, that were not previously seen. Increasing the number of hidden units does not necessarily improve the prediction on novel data. The situation is illustrated in Fig. 63 for the case of one input variable and one output variable. The crosses denote the data points that were used for training and the smooth curve is the neural network solution. For a small number of hidden units, the solution may look something like Fig. 63A. The solution does not pass through all the data points. For a larger number of hidden units, the solution may look something like Fig. 63B. The solution does pass through all the data points and is more complex. However, the prediction of the more complex network is less accurate than

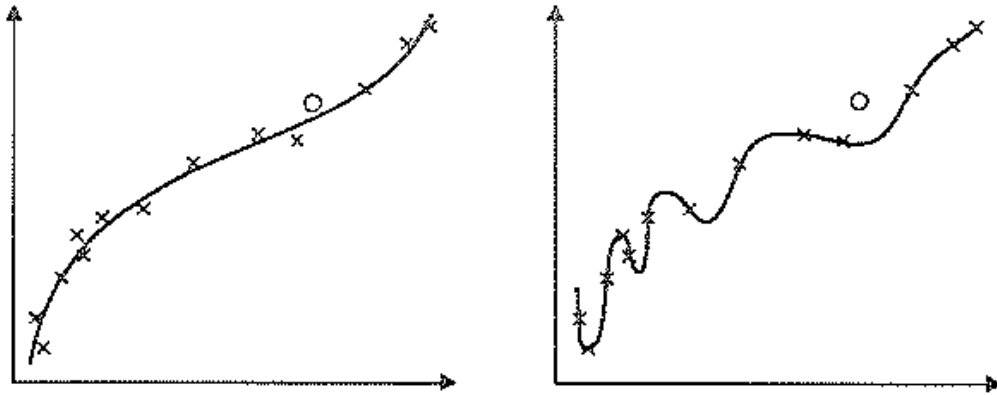


Figure 63: Network output versus network input. A) Network with a small number of hidden units. B) Network with a large number of hidden units. Networks with more hidden units can implement more complex functions and can better fit a given training set. However, more complex networks do not necessarily generalize better on novel data.

the simple network for the data point indicated by the circle, which was not part of the training set. The extend to which the trained neural network is capable of predicting on novel data is called the generalization performance. The network with the optimal generalization performance must balance two opposing criteria: minimization of the error on the training data requires a large number of hidden units, but the solution should also be sufficiently smooth to give good prediction.

6.7 Summary

This chapter is based on [12]. Perceptrons are simple models of feed-forward computation in a network of neurons. Binary perceptrons can be used for classification problems. Learning is done using the perceptron learning rule. The learning rule converges in a finite number of iterations if and only if the problem is linearly separable.

Perceptrons can also be constructed with continuous output, either using a linear or non-linear transfer function. These perceptrons can be learned using the gradient descent method. Gradient descent converges asymptotically for any data set.

The quality of the perceptron can be significantly improved by using multiple layers of hidden units. The multi-layered perceptron can learn any function by using a sufficiently large number of hidden units. However, prediction quality on novel data does not generally increase with the number of hidden units. Optimal generalization is obtained for a finite number of hidden units.

6.8 Exercises

1. Check dat $D_{max} = \frac{1}{\sqrt{3}}$ voor het AND probleem en $D_{max} = -\frac{1}{\sqrt{3}}$ voor het XOR probleem. Het AND probleem in de $\xi_i = \pm 1$ codering is gedefinieerd als $\zeta = 1$ als $\xi_1 = \xi_2 = 1$ and $\zeta = -1$ in alle overige gevallen. Het XOR probleem is gedefinieerd als $\zeta = \xi_1 * \xi_2$. Gebruik voor de gewichten vector $w = (w_0, w_1, w_2)$. (Hint: gebruik $w_1 = w_2$ vanwege symmetrie).
2. Beschouw gradient descent in een kostenlandschap gegeven door $E = a_1x^2 + a_2y^2$. Bereken de leerparameter η zodanig dat de convergentie in zowel x als y richting even snel is.
3. Beschouw een lineair perceptron (sectie 6.4) om de AND functie te leren.
 - wat zijn de optimale gewichten en drempels? wat is de optimale kosten E ?
 - laat zien dat $E > 0$ impliceert dat de inputpatronen lineair afhankelijk zijn.

4. Toon aan dat het gradient descent algoritme Eq. 31 asymptotisch convergeert.

References

- [1] D. Purves, G.J. Augustine, D. Fitzpatrick, L.C. Katz, A-S. LaMantia, and J.O. McNamara. *Neuroscience*. Sinauer associates, 1997.
- [2] A.L. Hodgkin and B. Katz. The effect of sodium ions on the electrical activity of the giant axon of the squid. *Journal of Physiology*, 108:37–77, 1949.
- [3] A.L. Hodgkin, A.F. Huxley, and B. Katz. Measurements of current-voltage relations in the membrane of the giant axon of *loligo*. *Journal of Physiology*, 116:424–448, 1952.
- [4] A.L. Hodgkin and A.F. Huxley. Currents carried by sodium and potassium ions through the membrane of a giant axon of *loligo*. *Journal of Physiology*, 116:449–472, 1952.
- [5] J.W. Moore, M.P. Blaustein, N.C. Anderson, and T. Narahashi. Basis of tetrodotoxin’s selectivity in blockage of squid axons. *Journal of General Physiology*, 50:1401–1411, 1967.
- [6] C.M. Armstrong and L. Binstock. Anomalous rectification in the squid giant axon injected with tetraethylammonium chloride. *Journal of General Physiology*, 48:859–872, 1965.
- [7] A.L. Hodgkin and A.F. Huxley. The components of membrane conductance in the giant axon of *loligo*. *Journal of Physiology*, 116:473–496, 1952.
- [8] B. Hille. *Ionic Channels of excitable membranes*. Sinaouer Associates, 1984.
- [9] B. Katz. *Nerve, muscle and synapse*. McGraw-Hill, 1966.
- [10] Chr. Koch. *Biophysics of computation*. Oxford University Press, 1999.
- [11] P. Peretto. *An introduction to the modeling of neural networks*. Cambridge University Press, 1992.
- [12] J. Hertz, A. Krogh, and R. Palmer. *Introduction to the theory of neural computation*, volume 1 of *Santa Fe Institute*. Addison-Wesley, Redwood City, 1991.